pharmaceuticals

MDPI

Article

Computer-Aided Design, Synthesis, and Antiviral Evaluation of Novel Acrylamides as Potential Inhibitors of E3-E2-E1 Glycoproteins Complex from Chikungunya Virus

Gabriel Felipe Silva Passos [1], Matheus Gabriel Moura Gomes [1], Thiago Mendonça de Aquino [2], João Xavier de Araújo-Júnior [1], Stephannie Janaina Maia de Souza [3], João Pedro Monteiro Cavalcante [3], Elane Conceição dos Santos [3], Ênio José Bassi [3] and Edeildo Ferreira da Silva-Júnior [1,2,*]

1 Laboratory of Medicinal Chemistry, Pharmaceutical Sciences Institute, Federal University of Alagoas, Maceió 57072-970, Brazil; gabrielfelipepassos@gmail.com (G.F.S.P.); matheus_gabriel199@hotmail.com (M.G.M.G.); jotaaraujo2004@gmail.com (J.X.d.A.-J.)

2 Center of Analysis and Research in Nuclear Magnetic Resonance, Chemistry and Biotechnology Institute, Federal University of Alagoas, Maceió 57072-970, Brazil; thiago.aquino@iqb.ufal.br

3 Immunoregulation Research Group, Laboratory of Research in Virology and Immunology, Institute of Biological and Health Sciences, Federal University of Alagoas, Maceió 57072-970, Brazil; stephanniemaia92@gmail.com (S.J.M.d.S.); j.p.monteirocavalcante@gmail.com (J.P.M.C.); elane.santos@icbs.ufal.br (E.C.d.S.); enio.bassi@icbs.ufal.br (Ê.J.B.)

* Correspondence: edeildo.junior@iqb.ufal.br; Tel.: +55-87-9-9610-8311

Received: 31 May 2020; Accepted: 25 June 2020; Published: 30 June 2020

Abstract: Chikungunya virus (CHIKV) causes an infectious disease characterized by inflammation and pain of the musculoskeletal tissues accompanied by swelling in the joints and cartilage damage. Currently, there are no licensed vaccines or chemotherapeutic agents to prevent or treat CHIKV infections. In this context, our research aimed to explore the potential in vitro anti-CHIKV activity of acrylamide derivatives. In silico methods were applied to 132 Michael's acceptors toward the six most important biological targets from CHIKV. Subsequently, the ten most promising acrylamides were selected and synthesized. From the cytotoxicity MTT assay, we verified that LQM330, 334, and 336 demonstrate high cell viability at 40 μM. Moreover, these derivatives exhibited anti-CHIKV activities, highlighting the compound LQM334 which exhibited an inhibition value of 81%. Thus, docking simulations were performed to suggest a potential CHIKV-target for LQM334. It was observed that the LQM334 has a high affinity towards the E3-E2-E1 glycoproteins complex. Moreover, LQM334 reduced the percentage of CHIKV-positive cells from 74.07 to 0.88%, 48h post-treatment on intracellular flow cytometry staining. In conclusion, all virtual simulations corroborated with experimental results, and LQM334 could be used as a promising anti-CHIKV scaffold for designing new drugs in the future.

Keywords: virtual screening; acrylamides; chikungunya virus; antiviral; molecular docking; E3-E2-E1 glycoproteins complex

1. Introduction

The Chikungunya virus (CHIKV) is an arbovirus from the *Alphavirus* genus, which belongs to the *Togaviridae* family [1,2]. It is mainly transmitted by the bite of infected mosquitoes from *Aedes aegypti* and *Ae. albopictus* species [3–8]; although, *Ae. furcifer* and *Culex* spp. mosquitoes have been also reported as vectors [3,9–11]. Since 1990, CHIKV infections have been reported in many countries from South and Central Americas, estimating 11,675 million cases [2,12–14]. Recently, it was verified that

the CHIKV is responsible for infecting people in more than 60 countries [15,16]. CHIKV is rarely fatal, whereas from 87 to 95% of infected patients are affected with debilitating arthralgia, swelling in the joints, and cartilage damage, in which these pathological conditions can persist for months or even years, in some cases [15]. Additionally, atypical cases involving complications associated with vision, cardiac, gastrointestinal, and neurological systems have been reported [17–19]. Moreover, Dengue (DENV) and/or Zika (ZIKV) patients co-infected by CHIKV have been described [20–22]. DENV and ZIKV are flaviviruses also transmitted by *Aedes* genus mosquitoes, which are associated with poverty and insufficient sanitation, being that DENV is a Neglected Tropical Disease (NTD), and CHIKV as well [23–25]. CHIKV is somewhat even more neglected than DENV [26,27].

Notwithstanding the high rates of CHIKV propagation, morbidity and mortality, there are no licensed vaccines or approved drugs to selectively treat this infectious disease [3,28,29]; although, research groups have reported the development of a new potential vaccine as a candidate for immunization against CHIKV [30]. Nowadays, the pharmacological treatment of CHIKV is limited to the antipyretic, analgesic, corticoid, and nonsteroidal anti-inflammatory drugs (NSAIDs) to relieve the typical symptoms [3,31].

The CHIKV genome comprises two open reading frames (ORFs), where a 5′ end ORF is capable of encoding four viral non-structural proteins (nsP1-nsP4), while a 3′ end ORF encodes viral structural proteins, which consist of capsid (C), two large enveloped glycoproteins (E1 and E2), and two accessory peptides (E3 and 6k) [32,33].

The nsP1 is involved in messenger RNA (mRNA) decoding and, via enzymatic activity of guanine-7-methyltransferase and guanylyltransferase, synthesis of viral negative single-stranded RNA [18,34–36]. In addition, the nsP2 has other essential enzymatic functions, which include RNA-helicase, nucleoside triphosphatase (NTPase), and RNA-dependent 5′-triphosphatase, where these are located in the *N*-terminal domain. In contrast, the *C*-terminal domain of nsP3 acts in part of the replicase and also as an accessory protein involved in the RNA synthesis [37–39]. Finally, the nsP4 acts as a RNA-dependent RNA-polymerase (RdRp) [18,38,40]. Differently, E1 and E2 proteins are responsible for spike glycoproteins in the surface from the viral particle, which facilitate the viral attachment to the susceptible host cells. The Ala/Val226 mutation in the E1 protein is associated with the generation of CHIKV-resistant strains [41,42]. Additionally, the Gly/Arg407 mutation in the E2 protein is responsible for generating CHIKV arbidol-resistant strains [43–45]. Typically, the CHIKV surface consists of 80 trimeric spikes composed of heterodimers of E1 and E2 proteins, in a lipid bilayer [46]. The CHIKV 6k is small, hydrophobic, and essential for the structural particle organization, in which it acts in the processing of sequence signaling of the E1 protein [46]. Nonetheless, the role of 6k in the CHIKV replication remains not fully understood [47].

Several in silico studies have identified that diverse chemical classes represent promising alternatives for the development of anti-CHIKV compounds, such as indoles [48], piperazines, benzimidazoles, pyrimidines [49], as well as phytocompounds [50]. Furthermore, studies involving organic synthesis have led to the obtainment of potential hit compounds, with low micromolar ranges. Among these, thiazolidine/rhodanine [51], peptidomimetic [52], thienopyrrole [53,54], triazolopyrimidinone [31], and adenosine analogs [55] have demonstrated excellent results. Therefore, one of the most promising chemical classes found in the literature is represented by acylhydrazone derivatives (and also acrylamide analogs), which have exhibited high activities with low cytotoxicity [56–59]. Essentially, the antiviral compounds can be categorized regarding their biological activity, being (*i*) CHIKV viral entry inhibitors [60,61]; (*ii*) nsP1 inhibitors [62]; (*iii*) nsP2 inhibitors [51,56–59]; (*iv*) nsP3 inhibitors [38]; (*v*) nsP4 inhibitors [63]; and (*vi*) viral RNA replication inhibitors [31,53,55,64,65]. In Figure 1, the best compounds found in the literature and their respective biological targets are illustrated. Finally, several other inhibitors targeting biological structures from CHIKV, as well as inhibitors with no specific targets can be found in the review manuscript by Silva-Júnior et al., (2017) [2].

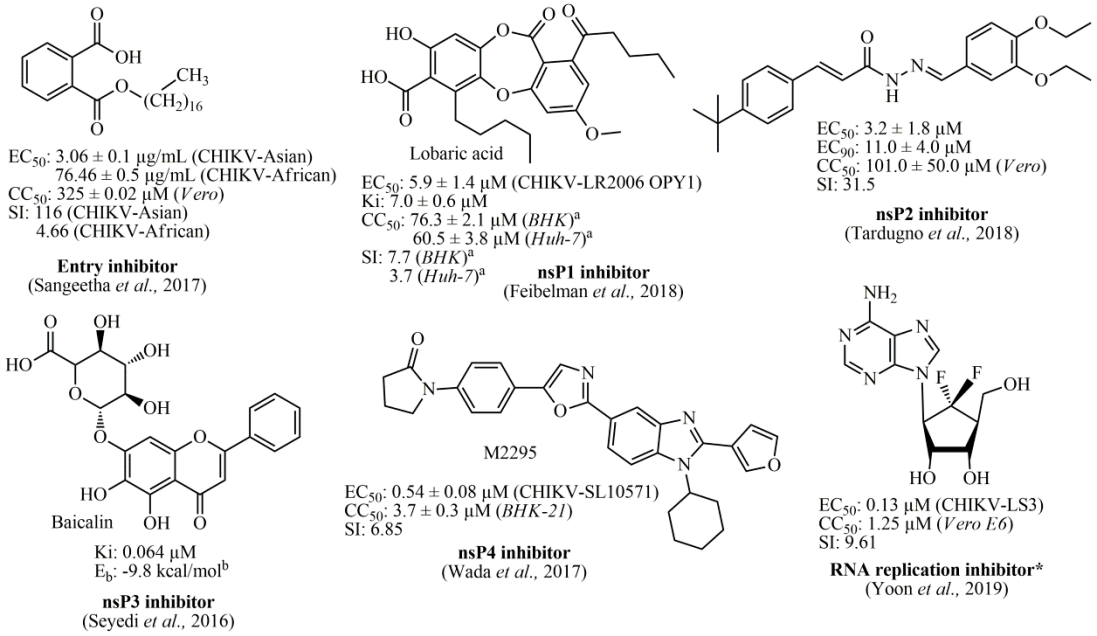

Figure 1. Best Chikungunya viral inhibitors reported in the literature and their corresponding targets. [a]: values obtained after 24 hours; [b]: Energy binding (E_b) value obtained by using Auto Dock Vina software; *: Fluorinated adenosine analog was reported as an RNA replication inhibitor, in which its antiviral activity was associated with an indirect effect on viral methyltransferase (MTase) activity through the inhibition of host S-adenosyl-$_L$-homocysteine (SAH) hydrolase.

In general, nsP2 inhibitors have been broadly explored by different research groups [51,56–59]. It is a cysteine protease that corresponds to approximately 20–30% of the viral particle, and also has four binding sites in its surface [1,52]. However, the binding site number 4 is considered the most important, since it contains the catalytic dyad, composed of Cys^{1013} and His^{1083} amino acids [49]. This cysteine protease has the potential to act as a nucleophile protein since the Cys^{1013} could be deprotonated by His^{1083}, via an acid-base mechanism, at physiological pH [49,66]. Therefore, Michael's acceptors represent an interesting alternative for developing anti-CHIKV compounds [56,58]. Additionally, the Trp^{1084} residue seems to perform an auxiliary role during the proteolytic activity of this protease [66]. As the global impacts of CHIKV and that the development of new antivirals is an unmet need, we aimed to develop new antiviral agents. The molecular docking of small flexible ligands toward macromolecules remains as the most broadly used in silico technique [67–71]. It is a stochastic method that uses scoring functions to find a minimum energy value, based on binding modes of ligands at the active site of macromolecules [72,73]. Essentially, it considers that hit compounds display high-affinity values forward their targets since they have favorable chemical groups for efficient interactions [69]. In this context, molecular docking was applied in this computer-guided study. Initially, virtual screening was performed in a dataset containing 132 compounds (including acrylamides and acylhydrazones) toward nsP2, nsP2/helicase, nsP3, immature and mature E3-E2-E1 glycoproteins complex, and C proteins. Meaningful FitScore values for acrylamide derivatives toward mature E3-E2-E1 glycoproteins complex were obtained by using molecular docking, which were analyzed by heat maps. Finally, an acrylamide analog exhibited a remarkable antiviral activity inhibiting the CHIKV infection in vitro, corroborating with our in silico results, suggesting that this compound acts by interaction with mature E3-E2-E1 glycoproteins complex and blocks the CHIKV attachment. Figure 2 presents the workflow including all the steps followed to perform this rational study.

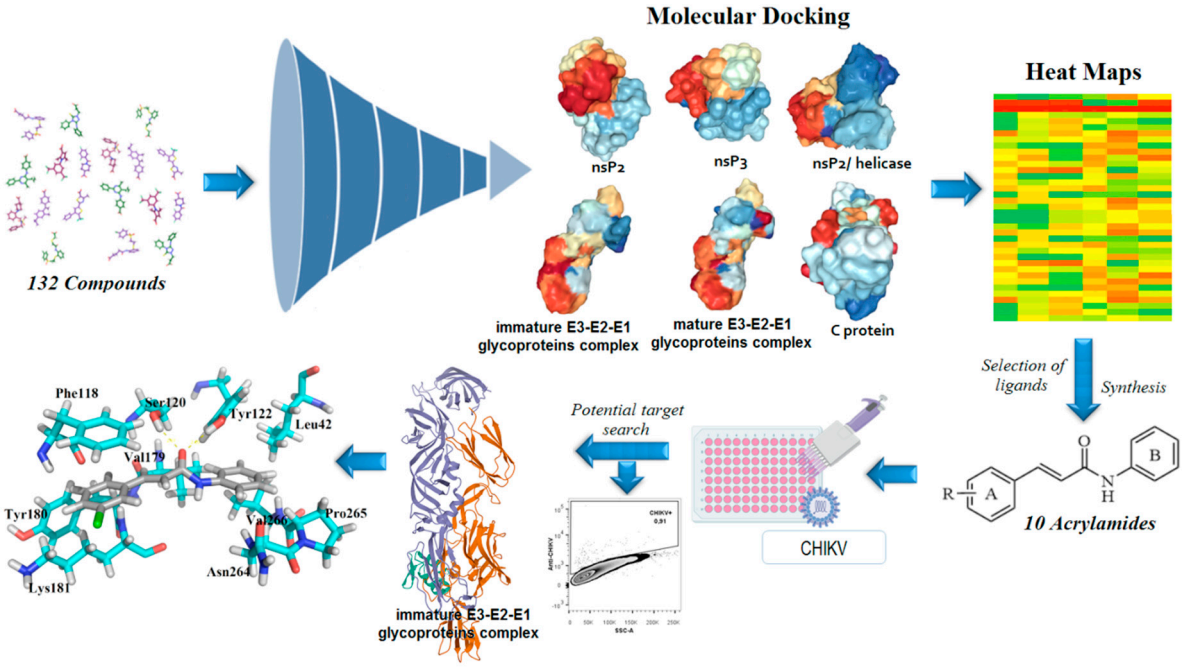

Figure 2. Workflow used to rationally develop acrylamides against the Chikungunya virus (CHIKV). In total, 132 compounds were analyzed toward nsP2 (Protein Data Bank (PDB): 3TRK), nsP2/helicase (PDB: 6JIM), nsP3 (PDB: 3GPO), immature E3-E2-E1 complex (PDB: 3N40), mature E3-E2-E1 complex (PDB: 3N41), and C (PDB: 5H23) proteins. Then, the most promising compounds were synthesized and screened. Lastly, the most active analog was docked into the E3-E2-E1 glycoproteins complex to identify the crucial amino acids involved in the ligand-target complex interactions.

2. Results and Discussion

2.1. Computer-Aided Drug Design

After the analysis of a dataset composed of 132 derivatives (including acrylamides and acylhydrazones) by molecular docking towards nsP2, nsP2/helicase, nsP3, immature and mature E3-E2-E1 glycoproteins complex, E, and C proteins from the CHIKV, it was identified that acrylamide derivatives could be more actives than acylhydrazones. In general, the 10 most favorable binding modes for each compound were generated by molecular docking. Moreover, it was verified that all molecules analyzed in this step demonstrated high affinity (FitScore) values forward the E3-E2-E1 glycoproteins complex (PDB ID: 3N41). Then, this observation was confirmed by using heat maps, in which a "hot-zone" was verified, concentrated on this molecular target. Thereafter, it was revealed that all acrylamides present FitScore values about 5–10 points higher than acylhydrazones. Additionally to this fact, some works have suggested that acylhydrazones and hydrazones could be associated with pan-assay interference scaffolds (PAINS), providing unreliable results in biological tests [74,75]. Combining this information and our virtual screening results, the top 10 most promising (FitScore $\geq$ 50.0) acrylamide derivatives (Figure 3) were selected for synthesis and biological evaluation in this study.

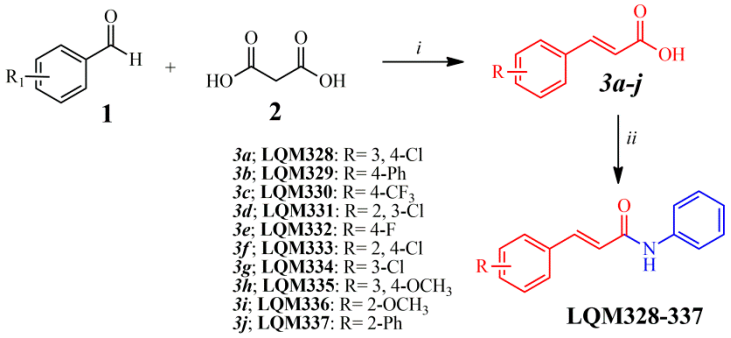

Figure 3. Synthetic route applied for the obtainment of acrylamide derivatives. Reagents and reactional conditions: (i) Pyridine, N-methylpiperazine (10 mol%), 24 hours, reflux; (ii) Aniline, dimethylformamide (DMF), 2-(1H-Benzotriazole-1-yl)-1,1′,3,3′-tetramethyluronium tetrafluoroborate (TBTU), diisopropylethylamine (DIPEA), 24 hours, at room temperature.

2.2. Chemistry

All the chemical intermediates (*3a-j*) were obtained by the reaction between corresponding aldehydes (1) and malonic acid (2), via Doebner–Knoevenagel condensation (Figure 3), with yields ranging from 45 to 94% [76,77]. Additionally, ^{1}H Nuclear Magnetic Resonance (NMR) spectra revealed that the intermediates (*3a-j*) were obtained in an (*E*)-configuration, confirmed by large vinylic coupling constant (*J*) values, ranging from 15.8 to 16.1 Hz [77,78]. Moreover, ^{1}H NMR analysis showed that the chemical shifts (δ) for the hydroxyl (OH) from the carboxylic acid can appear between 12.38 and 12.71 ppm. Subsequently, the acrylamide derivatives (LQM328-337) were obtained by the TBTU-coupling reaction (Figure 3), using diisopropylethylamine (DIPEA) as a catalyst base [79], with yields from 52 to 92%. For all these final compounds, the purity degree was determined by the HPLC technique, which resulted in purities ranging from 95.3 to 99.9%, with retention time (R_T) between 3.07 and 3.88 min. The analysis of Fourier-Transform Infrared (FT-IR) spectra revealed three characteristic stretches (υ) from these chemical molecules, ranging from 3240 to 3356 cm^{-1} for υ(N-H) bond; from 1658 to 1651 cm^{-1} for υ(C=O) bond; also from 1620 to 1612 cm^{-1} and from 979 to 964 cm^{-1} $\upsilon(C=C)_{ene}$ bond. Additionally, melting points (Mp) are uncorrected and they range from 113 to 227 °C. In the ^{1}H NMR spectra of the acrylamides, it was observed that the amide (N-H) signal ranges from 10.13 to 10.35 ppm. Equally to their intermediates, acrylamides were obtained in (*E*)-configuration, also confirmed by the vinylic coupling constant values, *J*. From ^{13}C NMR spectra, the carbonyl (C=O) from the amide group has chemical shifts (δ) varying from 163.17 to 164.42 ppm. Additionally, elemental analyses (CHN) were only performed for the new acrylamides synthesized (LQM328, LQM331, and LQM337), in which their chemical compositions ranging from 61.95 to 83.52% for carbon, from 3.96 to 5.68% for hydrogen, and from 4.67 to 4.94% for nitrogen. For all acrylamides previously synthesized, the corresponding references were provided in order to compare the results obtained in this study (see Materials and Methods section). Finally, all these physicochemical and spectroscopic techniques were sufficient to unequivocally characterize the compounds synthesized in this work. All chromatograms, FT-IR, ^{1}H and ^{13}C NMR spectra are available in the Supplementary Material related to this manuscript.

2.3. Cell Viability and Antiviral Assays

The cytotoxicity was performed in vitro for the ten synthesized acrylamides (LQM328 to LQM337) towards *Vero E6* cells at 20 μM concentration by MTT assay [80]. As shown in Figure 4, only the LQM329 was highly cytotoxic, reducing the cell viability to less than 50% (41.5% ± 3.3) after 48h of culture, thus being removed for further analysis. Therefore, the screening of antiviral activity against CHIKV was performed for all other nine acrylamides.

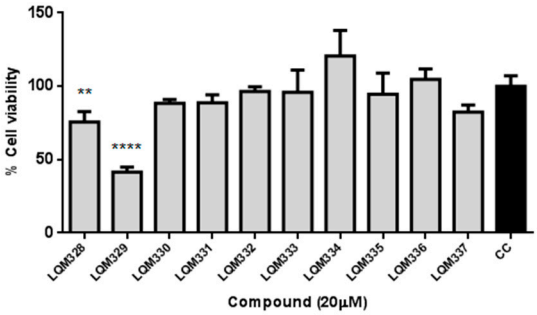

Figure 4. In vitro evaluation of cytotoxicity for synthesized acrylamides towards *Vero E6* cells. The cytotoxicity was performed in vitro for ten synthesized acrylamides (LQM328 to LQM337) towards *Vero E6* cells at 20 μM concentration by MTT assay after 48 h. The expressed values are results from mean ± SD of triplicates at 20 μM concentration, analyzed after 48 h. CC = cellular control. ** $p \leq 0.01$; **** $p \leq 0.0001$ versus CC.

Initially, the in vitro anti-CHIKV activity for the acrylamides was evaluated at a 20 μM concentration. For this purpose, CHIKV adsorption was performed in the *Vero E6* cells followed by the treatment with pre-selected compounds, and the cell viability was then assessed after 48h. As a result, significant viral inhibition was detected for the LQM328, LQM330, LQM334, LQM336, and LQM337 compounds (Figure 5).

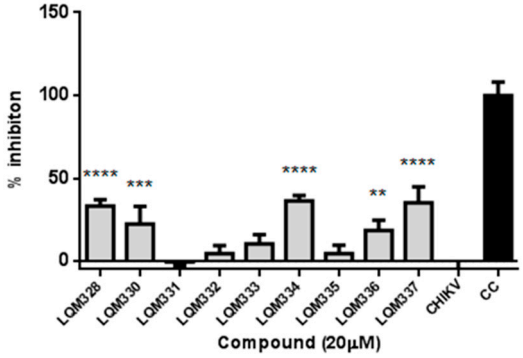

Figure 5. In vitro screening of anti-Chikungunya virus activity of acrylamides. The virus adsorption was performed for 2h followed by the addition of tested compounds at 20 μM concentration. The cell viability was assessed after 48h and the viral inhibition (%) was determined for each compound. The expressed values result from the mean ± SD of triplicates. CHIKV = CHIKV-infected untreated cells. CC = uninfected cellular control. ** $p \leq 0.01$; *** $p \leq 0.001$; **** $p \leq 0.0001$ versus CHIKV.

To investigate the improvement in the antiviral activity of the compounds due to a higher concentration of the compounds, both in vitro cytotoxicity and anti-CHIKV assays were evaluated at 40 μM concentration, after 72h for the five most promising acrylamides (LQM328, LQM330, LQM334, LQM336, and LQM337). Although high cytotoxicity was detected for the LQM328 and LQM337, no toxicity was detected for LQM330, LQM334, and LQM336 at this concentration (Figure 6A). Regarding anti-CHIKV activity, a significant viral inhibition was detected for LQM330, LQM334, and LQM336, with the highest antiviral activity detected for the LQM334 (viral inhibition = 81.1% ± 6.4 for LQM334 vs. 49.1% ± 11.1 for LQM330, and 32.2% ± 2.4 for LQM336), as shown in Figure 6B.

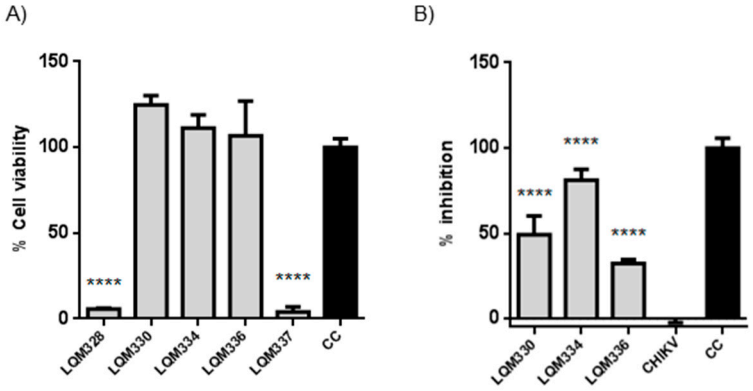

Figure 6. In vitro cytotoxicity and anti-Chikungunya virus results of acrylamides at 40 μM. (**A**) Evaluation of cytotoxicity for acrylamides in vitro towards *Vero E6* cells at 40 μM. The cytotoxicity was performed in vitro by MTT assay after 72h. **** $p \leq 0.0001$ versus CC. (**B**) Assessment of anti-CHIKV activity of acrylamides at 40 μM. The virus adsorption was performed for 2 h followed by the addition of tested compounds. The cell viability was assessed after 72 h and the viral inhibition (%) was determined for each compound. **** $p \leq 0.0001$ versus CHIKV. The expressed values result from the mean ± SD of triplicates. CHIKV = CHIKV-infected untreated cells. CC = uninfected cellular control.

2.4. Structure–Activity Relationship (SAR) Analysis

Posteriorly to the cell viability and antiviral assays, a structure–activity relationship (SAR) analysis was performed for this small series of acrylamide analogs (LQM328-337). As a rule, this will be discussed in the following sequence: electron-withdrawing; electron-donating; and aromatic ring substituents, considering the results at 20 and 40 μM, respectively.

Considering Figures 4 and 5, the analog containing trifluoromethyl substituent at position 4 (LQM330) presents good cell viability (88.3% ± 2.8) and viral inhibition activity value of 22.4% ± 10.6. When this group is replaced with a fluorine atom results in an analog (LQM332) with better cell viability (96.4% ± 3.3), however, it abolishes the antiviral effect. Considering the chloro-containing derivatives, it is verified that the chlorinated 2,3-disubstituted analog (LQM331) demonstrates good cell viability; in contrast, it is completely inactive. When the chlorine atom at position 3 is shifted to position 4, an analog (LQM333) non-cytotoxic and inactive against CHIKV is obtained. Moreover, when the chlorine atom is shifted from position 2 to 3, a derivative (LQM328) which is slightly more cytotoxic is generated, presenting a cell viability value of 75.5% ± 7.2. Additionally, a small improvement in the antiviral activity is observed, with an inhibition value of 33.1% ± 3.9. However, it is important to note that LQM328 was highly cytotoxic at 40 μM. Finally, when the chlorine atom at position 4 is removed, with only one remaining chlorine atom at position 3 (LQM334), the most active acrylamide is obtained, with a viral inhibition value of 36.3% ± 3.3 at 20 μM and 81.1% ± 6.4, at 40 μM concentration. Regarding the acrylamides containing electron-donating substituents, the 3,4-disubstituted methoxyl compound (LQM335) showed no cytotoxicity and it was not active against CHIKV. Furthermore, its analog substituted only at position 2 (LQM336) shows a slight antiviral activity at 20 μM (18.5% ± 6.1). Finally, the acrylamide derivative containing a phenyl ring as a substituent at position 4 (LQM329) has high cytotoxicity, exhibiting a poor cell viability value of 41.5% ± 3.3. When this phenyl group is shifted to position 2 (LQM337), its cytotoxicity at 20 μM is abolished.

Concerning the results at 40 μM concentration (Figure 6), it is possible to verify that the 3,4-disubstituted chlorine compound (LQM328) becomes highly toxic (5.7% ± 0.6), in comparison with its results at 20 μM. In contrast, when the chlorine atom is removed from position 4, the cell viability is strongly increased (LQM334). Additionally, the analog containing a 4-trifluoromethyl substituent (LQM330) exhibited good cell viability. Similarly, the compound with a strong electron-donating group, such as 2-methoxyl substituent (LQM336), shows good cell viability. In contrast, a phenyl ring at position 2 (LQM337) showed high cytotoxicity. Interestingly, compounds presenting electron-withdrawing

groups (LQM330 and 334) demonstrated better results in antiviral assays, with inhibition values of 49.1% ± 11.1 and 81.1% ± 6.4, respectively. Finally, LQM336 can be considered as a weak inhibitor against CHIKV, exhibiting an inhibition value of 32.2% ± 2.4, at 40 μM concentration.

In brief, Figure 7 summarizes the SAR analysis for the acrylamide derivatives at 20 μM, since the number of compounds was higher than those at 40 μM concentration.

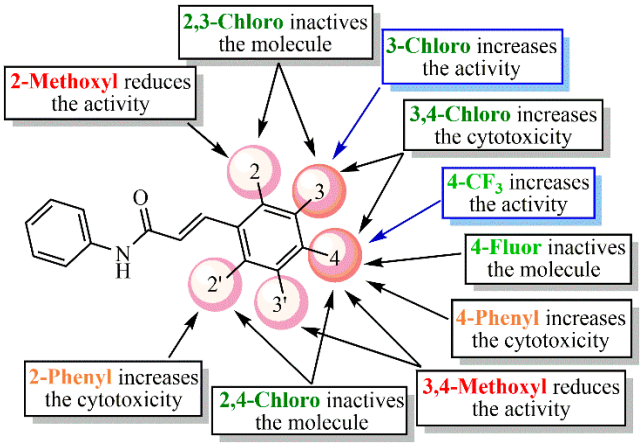

Figure 7. Summarization of structure–activity relationship (SAR) analysis for the acrylamides.

2.5. Intracellular Flow Cytometry Staining for CHIKV after Treatment with LQM334

In order to confirm the promising anti-CHIKV activity of LQM334, investigating its ability to inhibit the viral infection in *Vero E6* cells, the intracellular labeling of CHIKV was performed 48 h post-treatment and the percentage of CHIKV-positive cells was detected by flow cytometry. As shown in Figure 8A, LQM334 reduced the cytopathogenic effect induced by the virus compared to untreated cells (CHIKV). Moreover, LQM334 was able to significantly reduce the percentage of CHIKV-positive cells from 74.07% ± 1.19 to 7.38% ± 1.96 at 20 μM and to 0.88% ± 0.29 at 40 μM (Figure 8B,C).

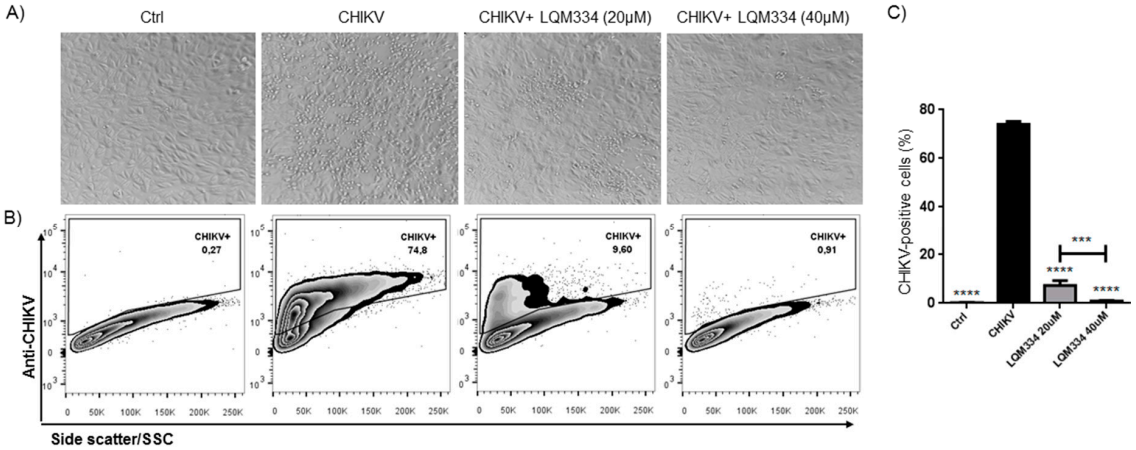

Figure 8. LQM334 inhibited the Chikungunya virus infection in vitro. In (**A**), Representative micrographs showing the cytopathogenic effect induced by the virus such as cell refringence changes and cell aggregates (200x magnification); In (**B**), Representative flow cytometry dot-plots of *Vero E6* cells infected (CHIKV) or uninfected (Control) with CHIKV. The cells were treated with LQM334 at 20 and 40 μM, respectively. The percentages of CHIKV-positive cells are shown; In (**C**), The expressed values are results from mean ± SD of triplicates. *** $p \leq 0.001$; **** $p \leq 0.0001$ versus untreated infected cells (CHIKV). CHIKV = CHIKV-infected untreated cells. Control/ctrl = uninfected cellular control.

2.6. Molecular Docking Studies for LQM334

After the obtainment of interesting results from the intracellular flow cytometry for the compound LQM334, a deep molecular docking analysis was performed throughout the possible six CHIKV targets, which were nsP2, nsP2/helicase, nsP3, immature and mature E3-E2-E1 glycoproteins complex, and C proteins. As a result, it was identified that LQM334 possibly binds more efficiently to the E2 domain A from the mature E3-E2-E1 glycoproteins complex (PDB: 3N41) (Figure 9A), exhibiting a FitScore value of 62.3293. Additionally, it is placed into the central cleft from the protein (Figure 9B). In order to obtain a FitScore parameter for comparison, the co-crystallized ligand from the mature E3-E2-E1 glycoproteins complex (a NAG molecule) was redocked using the same docking parameters, as described in methods' section. To validate this approach, the root-mean-square deviation (RMSD) was used to evaluate how different the obtained docking orientation is from the corresponding co-crystallized pose of the NAG molecule. Concerning docking solutions, RMSD values allow to classify them as: (*a*) good solution when RMSD ≤ 2.0 Å; (*b*) acceptable solutions when RMSD is between 2.0 and 3.0 Å, and (*c*) bad solutions when RMSD ≥ 3.0 Å [81–83]. As a result, an RMSD value of 1.132 Å was obtained for the NAG redocking solution, suggesting a reliable docking protocol. Then, it was revealed that NAG had a FitScore value of 46.4102, suggesting that the LQM334 has a high affinity to this CHIKV target. According to Voss et al. (2010), the NAG molecule hydrophobically interacts with Lys^{115}, Thr^{116}, Phe^{118}, Lys^{181}, Leu^{261}, Ala^{262}, and Asn^{263} amino acid residues [84]. Regarding these interactions, LQM334 also interacts with Phe^{118} and Lys^{181} residues. Still, it hydrophobically interacts with Leu^{42}, Val^{179}, Tyr^{180}, Asn^{264}, Pro^{265}, and Val^{266}, while also interacting with Ser^{120} and Tyr^{122} amino acids, via hydrogen bonding interactions at distances of 2.07 and 2.1 Å, respectively (Figure 9C). Additionally, in silico studies involving E3-E2-E1 glycoproteins have been developed focusing on virtual screening of phenothiazines, bafilomycin [85], and FAD-approved antimicrobial agents, such as cefmenoxime, ceforanide, cefotetan, cefonicid sodium, and cefpiramide [86]. Recently, Song et al. (2019) [87] reported the crystal structures of the free mouse MXRA8 (mMXR8) receptor and the complex between human MXRA8 (hMXRA8) and the CHIKV E3-E2-E1 glycoproteins complex. From this study, the authors verified that the interaction between hMXRA8 and E3-E2-E1 glycoproteins complex occurs via 25 hydrophobic contacts, including Asn^{264} and Pro^{265} residues, as observed for LQM334 interactions. This fact reinforces that LQM334 possibly binds to an important binding site in the E3-E2-E1 glycoproteins complex and thus, it could suggest this molecule as a potential virus entry inhibitor.

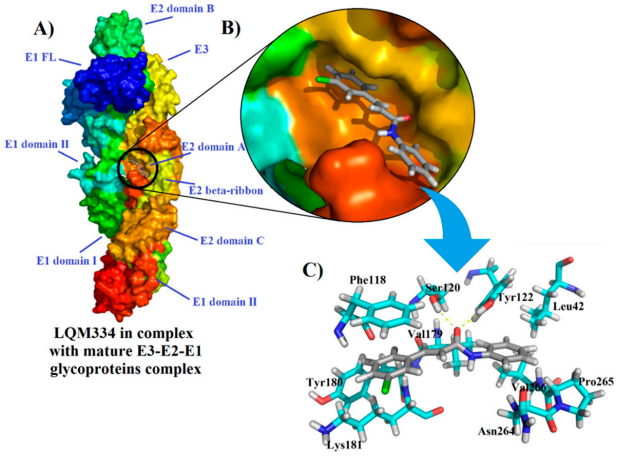

Figure 9. Interactions of LQM334 with mature E3-E2-E1 glycoproteins complex (PDB ID: 3N41) from the Chikungunya virus and its amino acids involved ligand-target complex. In (**A**), Overview of LQM334-mature E3-E2-E1 glycoproteins complex formation; In (**B**), Magnification showing the LQM334 into the central cleft from the glycoproteins complex; In (**C**), stick representations showing the amino acids involved in the complex formation with LQM334, in which yellow dots represent hydrogen bonding interactions.

3. Materials and Methods

3.1. Computational Details and Computer-Aided Drug Design

All in silico experiments involving molecular docking were performed in a Dell® notebook, (Texas, USA), model 5500U, with an Intel® Core™ 4th generation *i*-7 processer, CPU 2.4 GHz, 16 GB RAM, and running at Windows® 8.1 platform (Redmond, USA).

In total, 66 acrylamides and 66 acylhydrazones found in the literature were drawn, converted into three-dimensional structures, and energetically minimized by the application of the semi-empiric method Austin Model 1 (AM1), by using ArgusLab® software (Richland, USA), v. 4.0.1 (http://www.arguslab.com) [88]. Three-dimensional structures of nsP2 (PDB: 3TRK) [89], nsP2/helicase (PDB: 6JIM) [90], nsP3 (PDB: 3GPO) [91], immature E3-E2-E1 complex (PDB: 3N40) [84], mature E3-E2-E1 complex (PDB: 3N41) [84], and C (PDB: 5H23) [92] proteins were obtained at the Research Collaboratory for Structural Bioinformatics Protein Data Bank (RCSB PDB, San Diego, USA), website (https://www.rcsb.org). Pretreatment of these macromolecules and molecular docking simulations were performed using GOLD® software (Cambridge, UK), v. 5.8.1 (https://www.ccdc.cam.ac.uk/solutions/csd-discovery/components/gold/) [93]. Co-crystallized molecules from targets' structures were used for redocking in order to obtain FitScore cutoff values to build the virtual protocol. Subsequently, all these co-crystallized molecules were removed, including water molecules and ions. Then, H-bond acceptor and donor atoms were assumed as solvent accessible. Additionally, all four different scoring functions from GOLD® software were employed, being Chemical Piecewise Linear Potential (CHEMPLP), GoldScore, ChemScore, and Astex Statistical Potential (ASP). Finally, the correlation coefficient (r^2) for each scoring function was determined by the comparison between the redocked co-crystallized molecules and ligands in this study, acrylamides and acylhydrazones, using Microsoft Excel® 2010 to obtain useful heat maps (red and green mean hot and cold, respectively). Furthermore, all energetic contributions and interactions (H-bond, hydrophobic, and van der Waals) were individually analyzed. All illustrations were generated by using PyMol® software, v. 0.99 (https://pymol.org/2/). Lastly, all procedures performed in this study are in accordance with recently published works by our research team [94–100].

3.2. Reagents and Solvents

All starting reagents and solvents were purchased from Merck/Sigma-Aldrich® Company (St. Louis, MO, USA), and they were commercial products of high purity (>98%). Additionally, the solvents used in reactions and column chromatography were subjected to rotary evaporation before use to remove impurities. Finally, in high-performance liquid chromatography (HPLC) experiments, methanol HPLC degree from Tedia® High Purity Solvents Company (Fairfield, OH, USA) was used as eluent.

3.3. Chemical Characterization and Apparatus

For the intermediate products (3a-j), information about yields and physical aspects was provided. Additionally, these were only characterized by hydrogen Nuclear Magnetic Resonance (^{1}H NMR) since they are not new in the literature. For the final products (LQM328-LQM337), information about yields and physical aspects, purity, retention time (R_T), melting point (Mp) or degradation point (Dp), Fourier-Transform Infrared (FT-IR) spectra, ^{1}H and ^{13}C NMR spectra, and elemental analyses (CHN) were provided, since most of the final products are completely new in the literature. Finally, for the acrylamides previously synthesized, the corresponding references were also provided in this section.

3.4. High-Performance Liquid Chromatography—(HPLC)

For purity degree (%) and R_T determination for the final compounds, a Shimadzu® (Kyoto, Japan) chromatograph was used, model SIL-20AHT, utilizing a Luna® 5 µm C18(2) 100 Å column, with dimensions of 250 × 4.6 mm, and wavelength (λ) of 254 nm. All HPLC runs were performed using

methanol HPLC degree (≥99%) as a mobile phase. Moreover, some parameters were established, such as (a) sample concentration of 1 mg/mL; (b) flow of 1 mL/min; (c) run time of 15 min; and (d) injection volume of 5 µL. Finally, the retention times (R_T) were computed in minutes (min) and absorbance, in mili-absorbance unities (mAU) [101].

3.5. Melting Point Determination

All melting point (Mp) for final compounds were determined by using an MSTecnopon® (Piracicaba, Brazil), model PFMII Digital, with maximum temperature at 330 °C, utilizing glass capillaries containing the samples. Initially, 40 °C was admitted as a starting temperature and then a temperature increase by 1 °C/min was allowed. In some cases, Mp due to the degradation of the sample was not observed. Thus, the degradation point (Dp) was computed. Finally, all Mp or Dp are uncorrected and were assumed in a range of 1 °C between the values [102].

3.6. Fourier-Transform Infrared Spectroscopy–(FT-IR)

All FT-IR spectra were obtained using a spectrophotometer from Shimadzu® (Kyoto, Japan), model IRPrestige-21, employing the attenuated total reflectance (ATR) method, in the range from 4000 to 400 cm^{-1} [103,104]. All spectra were treated by using Shimadzu IRsolution® software, version 1.50, 2008. Finally, all bond stretches (v) and angle deformations (δ) for the main functional group from the final compounds (acrylamide moiety) were computed in transmittance (T%) and wavenumber (cm^{-1}) [105].

3.7. ^{1}H and ^{13}C Nuclear Magnetic Resonance Spectroscopy–(NMR)

All spectra of ^{1}H and ^{13}C NMR were obtained utilizing a Bruker® equipment (Billerica, USA), model UltraShield 600 MHz. Besides, deuterated methanol (MeOD), chloroform ($CDCl_3$), and dimethylsulfoxide (DMSO-d_6) were used as analytical solvents, depending on the samples' solubility. In total, it was admitted scans' number of 16 and 1024 for hydrogen and carbon nuclei, respectively. All chemical shifts were computed in part *per* millions (ppm). Additionally, coupling constants (J) were determined in hertz (Hz). Moreover, signal multiplicities were attributed as singlet (s), broad singlet (br s), doublet (d), double-doublets (dd), triplet (t), triplet of doublets (td), quartet (q), and multiplet (m) [78,106]. Finally, all NMR spectra were treated and analyzed by using the academic licensed Bruker TopSpin® software, version 4.0.7, 2019.

3.8. Elemental Analysis (CHN)

Samples containing 1–2 mg of LQM328, LQM331, and LQM337 were placed into tin capsules for solids, specific for elemental analyses. All determinations were carried out in a Perkin Elmer® equipment, model CHNS/O Analyzer 2400 series II. For combustion and reduction columns, the temperatures of 950 and 640 °C were used, respectively. Gas pressures for O_2 e He were admitted as 140 and 105 KPa, respectively. Additionally, a combustion column filling-time of 30 s was assumed. Finally, a total run-time of 5 min for each sample was allowed. These procedures are adaptations from works previously reported [107–109].

3.9. Synthesis of Cinnamic Acid and Acrylamide Derivatives

3.9.1. General Procedures for the Obtainment of Cinnamic Acids (3a-j)

In general, an adaptation of methods described by Luo and collaborators (2015) was used [110], through a Knoevenagel condensation Doebner modification reaction [77]. In a bottom flask (50 mL) containing 6 mL pyridine, the corresponding aldehydes (1.0 eq.) were added. Subsequently, malonic acid (1.1 eq.) was also added into the solution. After 15 min under reflux and stirring, *N*-methyl piperazine (10 mol%) was added as a catalyst base. Then, the reactional mixture was kept at these conditions overnight. After the reaction completion (verified by TLC), 10 mL distilled water was

added to the crude mixture, providing a white powder precipitated. The heterogeneous mixture was refrigerated (2 °C) by 30 min. Posteriorly, the mixture was stirred for 10 min and, then, 15 mL concentrated HCl (37%) was added into the flask until the pH of 1. Finally, the resulting precipitated was filtered and washed by distilled water (2 × 50 mL), affording the corresponding cinnamic acids.

(E)-3-(3,4-Dichlorophenyl)acrylic acid ***(3a)***

Yield: 60%. Aspect: white amorphous powder. ^{1}H NMR (600 MHz, MeOD) δ (ppm): 6.53 (*d*, 1H, CH_{ene}, *J* = 15.9 Hz), 7.53–7.55 (*m*, 2H, CH_{Ar}), 7.6 (*d*, 1H, CH_{ene}, *J* = 15.9 Hz), 7.79 (*s*, 1H, CH_{Ar}).

(E)-3-([1,1′-Biphenyl]-4-yl)acrylic acid ***(3b)***

Yield: 94%. Aspect: yellow amorphous powder. ^{1}H NMR (600 MHz, DMSO-d_6) δ (ppm): 6.58 (*d*, 1H, CH_{ene}, *J* = 15.9 Hz), 7.38 (*t*, 1H, CH_{Ar}, *J* = 7.3 Hz), 7.47 (*t*, 2H, CH_{Ar}, *J* = 7.6 Hz), 7.64 (*d*, 1H, CH_{ene}, *J* = 15.9 Hz), 7.7–7.72 (*m*, 4H, CH_{Ar}), 7.78 (*d*, 1H, CH_{Ar}, *J* = 8.2 Hz), 12.44 (*br s*, 1H, OH).

(E)-3-(4-(Trifluoromethyl)phenyl)acrylic acid ***(3c)***

Yield: 45%. Aspect: white amorphous powder. ^{1}H NMR (600 MHz, MeOD) δ (ppm): 6.48 (*d*, 1H, CH_{ene}, *J* = 16.0 Hz), 7.56 (*d*, 1H, CH_{Ar}, *J* = 8.0 Hz), 7.57 (*d*, 1H, CH_{ene}, *J* = 16.0 Hz), 7.65 (*d*, 1H, CH_{Ar}, *J* = 8.0 Hz), 8.05 (*d*, 1H, CH_{Ar}, *J* = 8.0 Hz).

(E)-3-(2,3-Dichlorophenyl)acrylic acid ***(3d)***

Yield: 78%. Aspect: white amorphous powder. ^{1}H NMR (600 MHz, DMSO-d_6) δ (ppm): 5.71 (*d*, 1H, CH_{ene}, *J* = 15.9 Hz), 6.53 (*t*, 1H, CH_{Ar}, *J* = 8.0 Hz), 6.77 (*dd*, 1H, CH_{Ar}, *J* = 8.0 and 1.5 Hz), 6.92 (*dd*, 1H, CH_{Ar}, *J* = 7.8 and 1.2 Hz), 7.24 (*d*, 1H, CH_{ene}, *J* = 15.9 Hz).

(E)-3-(4-Fluorophenyl)acrylic acid ***(3e)***

Yield: 80%. Aspect: white amorphous powder. ^{1}H NMR (600 MHz, DMSO-d_6) δ (ppm): 6.5 (*d*, 1H, CH_{ene}, *J* = 16.0 Hz), 7.25 (*t*, 2H, CH_{Ar}, *J* = 8.8 Hz), 7.59 (*d*, 1H, CH_{ene}, *J* = 15.9 Hz), 7.76–7.78 (*m*, 2H, CH_{Ar}), 12.41 (*br s*, 1H, OH).

(E)-3-(2,4-Dichlorophenyl)acrylic acid ***(3f)***

Yield: 65%. Aspect: white amorphous powder. ^{1}H NMR (600 MHz, DMSO-d_6) δ (ppm): 6.62 (*d*, 1H, CH_{ene}, *J* = 15.9 Hz), 7.45 (*dd*, 1H, CH_{Ar}, *J* = 8.4 and 2.1 Hz), 7.7 (*d*, 1H, CH_{Ar}, *J* = 2.0 Hz), 7.79 (*d*, 1H, CH_{ene}, *J* = 15.9 Hz), 7.94 (*d*, 1H, CH_{Ar}, *J* = 8.5 Hz), 12.71 (*br s*, 1H, OH).

(E)-3-(3-Chlorophenyl)acrylic acid ***(3g)***

Yield: 90%. Aspect: gray amorphous powder. ^{1}H NMR (600 MHz, DMSO-d_6) δ (ppm): 6.62 (*d*, 1H, CH_{ene}, *J* = 16.0 Hz), 7.42–7.47 (*m*, 2H, CH_{Ar}), 7.57 (*d*, 1H, CH_{ene}, *J* = 15.9 Hz), 7.67 (*d*, 1H, CH_{Ar}, *J* = 7.3 Hz), 7.78 (*s*, 1H, CH_{Ar}), 12.53 (*br s*, 1H, OH).

(E)-3-(3,4-Dimethoxyphenyl)acrylic acid ***(3h)***

Yield: 75%. Aspect: white amorphous powder. ^{1}H NMR (600 MHz, $CDCl_3$) δ (ppm): 3.93 (*s*, 6H, CH_3), 6.33 (*d*, 1H, CH_{ene}, *J* = 15.8 Hz), 6.89 (*d*, 1H, CH_{Ar}, *J* = 8.3 Hz), 7.08 (*d*, 1H, CH_{Ar}, *J* = 1.8 Hz), 7.15 (*dd*, 1H, CH_{Ar}, *J* = 8.3 and 1.8 Hz), 7.74 (*d*, 1H, CH_{ene}, *J* = 15.8 Hz).

(E)-3-(2-Methoxyphenyl)acrylic acid ***(3i)***

Yield: 90%. Aspect: white amorphous powder. ^{1}H NMR (600 MHz, MeOD) δ (ppm): 3.89 (*s*, 3H, CH_3), 6.5 (*d*, 1H, CH_{ene}, *J* = 16.1 Hz), 6.96 (*t*, 1H, CH_{Ar}, *J* = 7.3 Hz), 7.03 (*d*, 1H, CH_{ene}, *J* = 8.4 Hz), 7.37 (*td*, 1H, CH_{Ar}, *J* = 8.4, 1.5 and 1.3 Hz), 7.56 (*dd*, 1H, CH_{Ar}, *J* = 7.32 and 1.6 Hz), 7.97 (*d*, 1H, CH_{ene}, *J* = 16.1 Hz).

(E)-3-([1,1′-Biphenyl]-2-yl)acrylic acid ***(3j)***

Yield: 85%. Aspect: gray amorphous powder. ^{1}H NMR (600 MHz, DMSO-d_6) δ (ppm): 6.49 (*d*, 1H, CH_{ene}, *J* = 15.9 Hz), 7.31 (*d*, 2H, CH_{Ar}, *J* = 6.9 Hz), 7.36 (*d*, 1H, CH_{Ar}, *J* = 7.4 Hz), 7.42–7.45 (*m*, 2H, CH_{Ar}), 7.48–7.51 (*m*, 4H, CH_{Ar}), 7.9 (*d*, 1H, CH_{Ar}, *J* = 7.4 Hz), 12.38 (*br s*, 1H, OH).

3.9.2. General Procedures for the Obtainment of Acrylamides (LQM328–LQM337)

In general, an adaptation of methods described by Tanja and collaborators (2019) was used [79]. Initially, aniline (1.0 eq.) was added into a bottom flask (50 mL) containing 5 mL dimethylformamide (DMF) as the solvent. The corresponding cinnamic acid derivatives (1.1 eq.) were posteriorly added. Then, 2-(1*H*-Benzotriazole-1-yl)-1,1′,3,3′-tetramethyluronium tetrafluoroborate—TBTU (1.0 eq.) was

also added to the solution under stirring by 10 min. Subsequently, *N, N'*-diisopropylethylamine—DIPEA (3.5 eq.) was used added as a catalyst base. The reactional mixture remained under stirring and room temperature by 48 h. Then, 20 mL saturated $NaHCO_3$ solution (15 mL) was added to the crude mixture, providing a precipitate. This heterogeneous mixture was stirred for 15 min and, subsequently, the residual solid was filtered and washed with a saturated $NaHCO_3$ solution (3 × 10 mL) and, then, distilled water (3 × 25 mL), yielding the corresponding acrylamide derivatives. In some cases, it was necessary to further purifications. Lastly, these analogs were recrystallized from an acetone/water mixture (1:2), filtered and washed by distilled water (3 × 10 mL), providing pure products.

(E)-3-(3,4-Dichlorophenyl)-N-phenylacrylamide ***(LQM328)***

Yield: 55%. Aspect: yellow amorphous powder. Purity: 99.4%. R_T: 3.88 min. Mp. 145–146 °C. FT-IR (cm^{-1}): 3240 *v*(N-H), 1651 *v*(C=O), 1612 and 979 $v(C=C)_{ene}$. ^1H NMR (600 MHz, DMSO-d_6) δ (ppm): 6.89 (*d*, 1H, CH_{ene}, *J* = 15.7 Hz), 7.08 (*t*, 1H, CH_{Ar}, *J* = 7.3 Hz), 7.34 (*t*, 2H, CH_{Ar}, *J* = 7.9 Hz), 7.57 (*d*, 1H, CH_{ene}, *J* = 15.7 Hz), 7.63 (*dd*, 1H, CH_{Ar}, *J* = 8.3 and 1.9 Hz), 7.7 (*t*, 3H, CH_{Ar}, *J* = 8.3 Hz), 7.9 (*d*, 1H, CH_{Ar}, *J* = 1.9 Hz), 10.24 (*br s*, 1H, NH). ^{13}C NMR (150 MHz, DMSO-d_6) δ (ppm): 119.74, 123.99, 125.15, 127.86, 129.29, 130.06, 131.61, 132.22, 132.35, 136.17, 137.9, 139.55, 163.5. $CHN_{calculed}$ (%) for $C_{15}H_{11}Cl_2NO$: C 61.67, H 3.8, N 4.79. CHN_{found} (%): C 61.95, H 3.96, N 4.94.

(E)-3-([1,1'-Biphenyl]-4-yl)-N-phenylacrylamide ***(LQM329)***

Yield: 52%. Aspect: white amorphous powder. Purity: 97.7%. R_T: 3.52 min. Mp: 226–227 °C. FT-IR (cm^{-1}): 3309 *v*(N-H), 1658 *v*(C=O), 1620 and 972 $v(C=C)_{ene}$. ^1H NMR (600 MHz, DMSO-d_6) δ (ppm): 6.89 (*d*, 1H, CH_{ene}, *J* = 15.6 Hz), 7.07 (*t*, 1H, CH_{Ar}, *J* = 7.3 Hz), 7.34 (*t*, 2H, CH_{Ar}, *J* = 7.8 Hz), 7.39 (*t*, 1H, CH_{Ar}, *J* = 7.3 Hz), 7.48 (*t*, 2H, CH_{Ar}, *J* = 7.6 Hz), 7.63 (*d*, 1H, CH_{ene}, *J* = 15.6 Hz), 7.71 (*d*, 6H, CH_{Ar}, *J* = 7.8 Hz), 7.76 (*d*, 2H, CH_{Ar}, *J* = 8.2 Hz), 10.23 (*br s*, 1H, NH). ^{13}C NMR (150 MHz, DMSO-d_6) δ (ppm): 119.72, 122.75, 123.83, 127.1, 127.67, 128.34, 128.83, 129.27, 129.49, 134.34, 139.76, 140.1, 141.75, 164.02.

Reference: Carissimi (1959) [111].

(E)-N-Phenyl-3-(4-(trifluoromethyl)phenyl)acrylamide ***(LQM330)***

Yield: 87%. Aspect: white amorphous powder. Purity: 96.5%. R_T: 3.23 min. Mp: 154–155 °C. FT-IR (cm^{-1}): 3356 *v*(N-H), 1651 *v*(C=O), 1620 and 972 $v(C=C)_{ene}$. ^1H NMR (600 MHz, DMSO-d_6) δ (ppm): 6.97 (*d*, 1H, CH_{ene}, *J* = 15.7 Hz), 7.09 (*t*, 1H, CH_{Ar}, *J* = 7.3 Hz), 7.35 (*t*, 2H, CH_{Ar}, *J* = 7.8 Hz), 7.67 (*d*, 1H, CH_{ene}, *J* = 15.7 Hz), 7.7 (*d*, 2H, CH_{Ar}, *J* = 7.8 Hz), 7.81 (*d*, 2H, CH_{Ar}, *J* = 8.4 Hz), 7.85 (*d*, 2H, CH_{Ar}, *J* = 8.2 Hz), 10.31 (*br s*, 1H, NH). ^{13}C NMR (150 MHz, DMSO-d_6) δ (ppm): 119.76, 124.03, 125.47, 125.63, 126.36, 128.79, 129.31, 138.84, 139.29, 139.56, 163.49.

Reference: Guo et al. (2012) [112].

(E)-3-(2,3-Dichlorophenyl)-N-phenylacrylamide ***(LQM331)***

Yield: 90%. Aspect: white amorphous powder. Purity: 99.3%. R_T: 3.48 min. Mp: 212–213 °C. FT-IR (cm^{-1}): 3255 *v*(N-H), 1651 *v*(C=O), 1620 and 964 $v(C=C)_{ene}$. ^1H NMR (600 MHz, DMSO-d_6) δ (ppm): 6.89 (*d*, 1H, CH_{ene}, *J* = 15.5 Hz), 7.08 (*t*, 1H, CH_{Ar}, *J* = 7.08 Hz), 7.34 (*t*, 2H, CH_{Ar}, *J* = 7.8 Hz), 7.46 (*t*, 1H, CH_{Ar}, *J* = 7.9 Hz), 7.69 (*d*, 2H, CH_{Ar}, *J* = 7.9 Hz), 7.72 (*d*, 2H, CH_{Ar}, *J* = 7.8 Hz), 7.87 (*d*, 1H, CH_{ene}, *J* = 15.6 Hz), 10.35 (*br s*, 1H, NH). ^{13}C NMR (150 MHz, DMSO-d_6) δ (ppm): 119.82, 124.13, 126.82, 127.31, 129.11, 129.32, 131.69, 131.73, 133.08, 135.69, 135.76, 139.45, 163.17. $CHN_{calculed}$ (%) for $C_{15}H_{11}Cl_2NO$: C 61.67, H 3.8, N 4.79. CHN_{found} (%): C 62.21, H 3.75, N 4.67.

(E)-3-(4-Fluorophenyl)-N-phenylacrylamide ***(LQM332)***

Yield: 81%. Aspect: white amorphous powder. Purity: 99.4%. R_T: 3.16 min. Mp: 135–136 °C. FT-IR (cm^{-1}): 3309 *v*(N-H), 1658 *v*(C=O), 1620 and 964 $v(C=C)_{ene}$. ^1H NMR (600 MHz, DMSO-d_6) δ (ppm): 6.77 (*d*, 1H, CH_{ene}, *J* = 15.7 Hz), 7.06 (*t*, 1H, CH_{Ar}, *J* = 7.3 Hz), 7.28 (*t*, 2H, CH_{Ar}, *J* = 8.7 Hz), 7.33 (*t*, 2H, CH_{Ar}, *J* = 7.8 Hz), 7.58 (*d*, 1H, CH_{ene}, *J* = 15.7 Hz), 7.67–7.7 (*m*, 4H, CH_{Ar}), 10.2 (*br s*, 1H, NH). ^{13}C NMR (150 MHz, DMSO-d_6) δ (ppm): 116.39, 119.72, 122.69, 123.83, 129.25, 130.33, 131.85, 139.39, 139.71, 162.51, 163.92.

Reference: Sethiya et al. (2019) [113].

(E)-3-(2,4-Dichlorophenyl)-N-phenylacrylamide ***(LQM333)***

Yield: 92%. Aspect: white amorphous powder. Purity: 99.4%. R_T: 3.63 min. Mp: 180–181 °C. FT-IR (cm^{-1}): 3278 *v*(N-H), 1651 *v*(C=O), 1620 and 964 $v(C=C)_{ene}$. ^1H NMR (600 MHz, DMSO-d_6) δ (ppm): 6.9 (*d*, 1H, CH_{ene}, *J* = 15.6 Hz), 7.08 (*t*, 1H, CH_{Ar}, *J* = 7.3 Hz), 7.34 (*t*, 2H, CH_{Ar}, *J* = 7.8 Hz), 7.53 (*dd*, 1H, CH_{Ar}, *J* = 8.4 and 1.8 Hz), 7.7 (*d*, 2H, CH_{Ar}, *J* = 8.0 Hz), 7.74 (*d*, 1H, CH_{Ar}, *J* = 2.0 Hz), 7.77 (*d*, 1H, CH_{Ar}, *J* = 8.5 Hz), 7.79 (*d*, 1H, CH_{ene}, *J* = 15.6 Hz), 10.32 (*br s*, 1H, NH). ^{13}C NMR (150 MHz, DMSO-d_6) δ (ppm): 119.78, 124.09, 126.56, 128.61, 129.31, 129.41, 129.99, 132.12, 134.6, 134.68, 135.2, 139.47, 163.25.

Reference: Qiu and Zhang (2014) [114].

(E)-3-(3-Chlorophenyl)-N-phenylacrylamide ***(LQM334)***

Yield: 81%. Aspect: brown amorphous powder. Purity: 99.9%. R_T: 3.58 min. Mp: 123–124 °C. FT-IR (cm^{-1}): 3278 *v*(N-H), 1651 *v*(C=O), 1620 and 964 $v(C=C)_{ene}$. ^1H NMR (600 MHz, DMSO-d_6) δ (ppm): 6.89 (*d*, 1H, CH_{ene}, *J* = 15.7 Hz), 7.08 (*t*, 1H, CH_{Ar}, *J* = 7.3 Hz), 7.34 (*t*, 2H, CH_{Ar}, *J* = 7.8 Hz), 7.47–7.49 (*m*, 2H, CH_{Ar}), 7.58 (*d*, 1H, CH_{ene}, *J* = 15.7 Hz), 7.59–7.61 (*m*, 1H, CH_{Ar}), 7.69–7.1 (*m*, 3H, CH_{Ar}), 10.23 (*br s*, 1H, NH). ^{13}C NMR (150 MHz, DMSO-d_6) δ (ppm): 119.73, 123.95, 124.56, 126.61, 127.84, 129.28, 129.81, 131.3, 134.2, 137.54, 138.94, 139.6, 163.64.

Reference: Frei et al. (2017) [115].

(E)-3-(3,4-Dimethoxyphenyl)-N-phenylacrylamide ***(LQM335)***

Yield: 72%. Aspect: white amorphous powder. Purity: 99.5%. R_T: 3.07 min. Mp: 130–131 °C. FT-IR (cm^{-1}): 3309 *v*(N-H), 1651 *v*(C=O), 1620 and 964 $v(C=C)_{ene}$. ^1H NMR (600 MHz, DMSO-d_6) δ (ppm): 3.8 (*s*, 3H, CH_3), 3.82 (*s*, 3H, CH_3), 6.71 (*d*, 1H, CH_{ene}, *J* = 15.6 Hz), 7.01 (*d*, 1H, CH_{Ar}, *J* = 8.2 Hz), 7.05 (*t*, 1H, CH_{Ar}, *J* = 7.3 Hz), 7.19 (*dd*, 1H, CH_{Ar}, *J* = 8.2 and 1.5 Hz), 7.22 (*d*, 1H, CH_{Ar}, *J* = 1.5 Hz), 7.33 (*t*, 2H, CH_{Ar}, *J* = 7.8 Hz), 7.53 (*d*, 1H, CH_{ene}, *J* = 15.6 Hz), 7.7 (*d*, 2H, CH_{Ar}, *J* = 7.8 Hz), 10.13 (*br s*, 1H, NH). ^{13}C NMR (150 MHz, DMSO-d_6) δ (ppm): 55.88, 56.04, 110.48, 112.25, 119.57, 120.35, 122.25, 123.63, 127.96, 129.24, 139.91, 140.73, 149.4, 150.86, 164.31.

Reference: Araújo-Vilges et al. (2017) [116].

(E)-3-(2-Methoxyphenyl)-N-phenylacrylamide ***(LQM336)***

Yield: 90%. Aspect: white amorphous powder. Purity: 99.2%. R_T: 3.11 min. Mp: 136–137 °C. FT-IR (cm^{-1}): 3286 *v*(N-H), 1651 *v*(C=O), 1620 and 972 *v*(C=C)ene. ^1H NMR (600 MHz, DMSO-d_6) δ (ppm): 3.88 (*s*, 3H, CH_3), 6.88 (*d*, 1H, CH_{ene}, *J* = 15.8 Hz), 7.01 (*t*, 1H, CH_{Ar}, *J* = 7.4 Hz), 7.05 (*t*, 1H, CH_{Ar}, *J* = 7.3 Hz), 7.09 (*d*, 1H, CH_{Ar}, *J* = 8.3 Hz), 7.32 (*t*, 2H, CH_{Ar}, *J* = 7.7 Hz), 7.39 (*t*, 1H, CH_{Ar}, *J* = 7.7 Hz), 7.57 (*d*, 1H, CH_{Ar}, *J* = 7.4 Hz), 7.7 (*d*, 2H, CH_{Ar}, *J* = 7.9 Hz), 7.81 (*d*, 1H, CH_{ene}, *J* = 15.7 Hz), 10.18 (*br s*, 1H, NH). ^{13}C NMR (150 MHz, DMSO-d_6) δ (ppm): 56.09, 112.25, 119.5, 121.23, 123.1, 123.54, 123.72, 128.69, 129.24, 131.66, 135.78, 139.58, 158.2, 164.42.

Reference: Ittyerah and Pandya (1941) [117], and Yamamori et al. (2004) [118].

(E)-3-([1,1′-Biphenyl]-2-yl)-N-phenylacrylamide ***(LQM337)***

Yield: 84%. Aspect: brown amorphous powder. Purity: 95.3%. R_T: 3.38 min. Mp: 194–195 °C. FT-IR (cm^{-1}): 3255 *v*(N-H), 1651 *v*(C=O), 1620 and 972 $v(C=C)_{ene}$. ^1H NMR (600 MHz, DMSO-d_6) δ (ppm): 6.84 (*d*, 1H, CH_{ene}, *J* = 15.5 Hz), 7.05 (*t*, 1H, CH_{Ar}, *J* = 7.3 Hz), 7.3–7.34 (*m*, 4H, CH_{Ar}), 7.43–7.46 (*m*, 2H, CH_{Ar}), 7.49–7.51 (*m*, 5 H, CH_{Ar} and CH_{ene}), 7.66 (*d*, 2H, CH_{Ar}, *J* = 7.85 Hz), 7.78–7.8 (*m*, 1H, CH_{Ar}), 10.22 (*br s*, 1H, NH). ^{13}C NMR (150 MHz, DMSO-d_6) δ (ppm): 119.65, 123.63, 123.83, 126.73, 128.01, 128.46, 128.88, 129.24, 130.06, 130.25, 130.91, 132.91, 139.02, 139.67, 140.18, 142.6, 163.85. $CHN_{calculed}$ (%) for $C_{21}H_{17}NO$: C 84.25, H 5.72, N 4.68. CHN_{found} (%): C 83.52, H 5.68, N 4.81.

3.10. Cell Viability Assay

Briefly, *Vero E6* cells were plated at 2×10^4 cells/well in 96-well microplate and cultured in at 37 °C and 5% CO_2 atmosphere. Confluent cells monolayers were cultured in DMEM-low glucose (Sigma-Aldrich®, St. Louis, MO, USA) with 2% fetal bovine serum (Gibco) and antibiotic antimycotic solution (Gibco), for 48h or 72h in the presence of acrylamides at 20 or 40 µM. The cell viability was then evaluated using MTT (3-(4,5-Dimethyl-2-thiazolyl)-2,5-diphenyl-2H-tetrazolium (Sigma-Aldrich®, St. Louis, MO, USA) cytotoxic assay [80]. Therefore, the MTT solution was added at a final concentration

of 0.5 mg/mL followed by incubation for 3h. The culture medium was removed and 150 µL of dimethyl sulfoxide (DMSO) was added to each well leading to formazan solubilization. The value of blank control absorbance (only the used culture medium in the absence of cells) was subtracted from all samples. The absorbance of each well was measured at a 492 nm wavelength and the percentage of cell viability was calculated as follows:

$$\textit{Cell viability (\%) = [sample absorbance/average of cell control absorbance]} \times 100. \quad (1)$$

3.11. In Vitro Antiviral Assay

Initially, a serial dilution of CHIKV stock was performed and the viral dilution that has been reduced cell viability at least 80% was used in antiviral assays (data not shown). After that, *Vero E6* cells were plated at 2×10^4 cells/well in a 96-well microplate and maintained at 37 °C and 5% CO_2 atmosphere until reaching the confluence of ~80–90%. The virus adsorption was then performed by incubating the cells with CHIKV diluted 1:200 in DMEM-low glucose medium/2% bovine fetal serum for 2 h with homogenization every 15 min. Thereafter, the medium was removed and the cellular monolayers were washed with phosphate-buffered saline, and several synthesized acrylamides were added at 20 or 40 µM. The cell viability was assessed after 48 or 72 h by MTT cell viability assay as previously described (topic 3.9). The percentage of viral inhibition was calculated as follows:

$$\textit{Inhibition (\%) = [sample absorbance} - \textit{average of viral control absorbance/average of} \quad (2)$$

$$\textit{cellular control absorbance} - \textit{average of viral control absorbance]} \times 100.$$

3.12. Intracellular Flow Cytometry Staining for CHIKV

The antiviral activity of the LQM334 compound was confirmed by intracellular flow cytometry staining [119]. Briefly, after CHIKV adsorption in *Vero E6* cells for 2 h, the medium was removed, the cell monolayer was washed with PBS. The LQM334 compound was added at 20 or 40 µM concentrations and the cells were maintained at 37 °C/5% CO_2 atmosphere for 48h. The cells were detached by using a trypsin/EDTA solution and submitted to fixation and permeabilization using the BD Cytofix/Cytoperm™ Fixation/Permeabilization solution kit (BD Biosciences®, San Jose, CA, USA) according to the manufacturer's recommendations. Subsequently, the cells were incubated with an anti-CHIKV monoclonal antibody (1:50; A54Q clone; Invitrogen, Carlsbad, CA, USA) for 1h at 4 °C. The cells were washed with the BD Perm Wash solution (BD Biosciences®, San Jose, CA, USA) and then incubated with the goat anti-mouse IgG (H + L) cross-adsorbed secondary antibody conjugated with Alexa Fluor 488 (1:200; Invitrogen) for 1h at 4 °C. A total of 20,000 events were acquired in the BD FACS Canto™ II flow cytometer (BD Biosciences®, San Jose, CA, USA) and the results were analyzed by using FlowJo™ v. 10 software.

3.13. Statistical Analysis

The statistical analyses were performed in the GraphPad Prism® v.6.0 software (San Diego, CA, USA) using One-Way ANOVA followed by Dunnett multiple comparison tests, and the $p \leq 0.05$ was considered statistically significant.

4. Conclusions

A dataset of 132 compounds (including acrylamides and acylhydrazones) was built for a virtual protocol. Then, the computer-aided drug design protocol applied towards six CHIKV targets was able to identify 10 promising acrylamides to be synthesized and biologically evaluated. In the cytotoxicity assay, nine of 10 synthesized compounds presented a cell viability higher than 75%, at 20 µM concentration, with promising results in regards to the challenge in infected *Vero E6* cells with CHIKV. As a result, the compound LQM334 was found to be the most active analog, even though in a

higher concentration, it kept the cell viability and viral inhibition. Additionally, the intracellular flow cytometry staining demonstrated that LQM334 inhibited cell infection by the CHIKV. Regarding the antiviral activity of LQM334, the deep molecular docking analysis pointed to a possible virus target for LQM334. In this regard, it was identified that LQM334 preferably interacts with the E2 domain A from the mature E3-E2-E1 glycoproteins complex from CHIKV. Additionally, it displays hydrogen bonding interactions with Ser^{120} and Tyr^{122} amino acid residues. Therefore, our virtual pipeline pointed out a potential inhibitor of E3-E2-E1 glycoproteins complex from CHIKV with antiviral activity. It suggests that the medicinal chemistry of CHIKV should be more explored in order to provide more information about the most relevant chemical classes of compounds for designing new antiviral agents. Finally, this work represents the emergence of a new potential E3-E2-E1 glycoprotein complex inhibitor, which is in continuous development and several structural optimizations are being performed currently in order to identify new potent candidates with low toxicity. Concerning all of the results for LQM334, it is possible to suggest that this acrylamide analog could be used as a promising anti-CHIKV scaffold for the design of new antiviral agents in the future.

Supplementary Materials: The following are available online at http://www.mdpi.com/1424-8247/13/7/141/s1, **Figure S1**. *^{1}H NMR spectrum of (E)-3-(3,4-Dichlorophenyl)acrylic acid* (3a), **Figure S2**. *^{1}H NMR spectrum of (E)-3-([1,1′-Biphenyl]-4-yl)acrylic acid* (3b), **Figure S3**. *^{1}H NMR spectrum of (E)-3-(4-(Trifluoromethyl)phenyl)acrylic acid* (3c), **Figure S4**. *^{1}H NMR spectrum of (E)-3-(2,3-Dichlorophenyl)acrylic acid* (3d), **Figure S5**. *^{1}H NMR spectrum of (E)-3-(4-Fluorophenyl)acrylic acid* (3e), **Figure S6**. *^{1}H NMR spectrum of (E)-3-(2,4-Dichlorophenyl)acrylic acid* (3f), **Figure S7**. *^{1}H NMR spectrum of (E)-3-(3-Chlorophenyl)acrylic acid* (3g), **Figure S8.** *^{1}H NMR spectrum of (E)-3-(3,4 -Dimethoxyphenyl)acrylic acid* (3h), **Figure S9**. *^{1}H NMR spectrum of (E)-3-(2-Methoxyphenyl)acrylic acid* (3i), **Figure S10**. *^{1}H NMR spectrum of (E)-3-([1,1′-Biphenyl]-2-yl)acrylic acid* (3j), **Figure S11**. *HPLC chromatogram of (E)-3-(3,4 -Dichlorophenyl)-N-phenylacrylamide* (LQM328), **Figure S12**. *FT-IR spectrum of (E)-3-(3,4-Dichlorophenyl) -N-phenylacrylamide* (LQM328), **Figure S13**. *^{1}H NMR spectrum of (E)-3-(3,4-Dichlorophenyl)-N-phenylacrylamide* (LQM328), **Figure S14**. *^{13}C NMR spectrum of (E)-3-(3,4-Dichlorophenyl)-N-phenylacrylamide* (LQM328), **Figure S15.** *HPLC chromatogram of (E)-3-([1,1′-Biphenyl]-4-yl)-N-phenylacrylamide* (LQM329), **Figure S16**. *FT-IR spectrum of (E)-3-([1,1′ -Biphenyl]-4-yl)-N-phenylacrylamide* (LQM329), **Figure S17**. *^{1}H NMR spectrum of (E)-3-([1,1′-Biphenyl]-4 -yl)-N-phenylacrylamide (LQM329),* **Figure S18**. *^{13}C NMR spectrum of (E)-3-([1,1′-Biphenyl]-4-yl)-N-phenylacrylamide (LQM329),* **Figure S19.** *HPLC chromatogram of (E)-N-Phenyl-3-(4-(trifluoromethyl)phenyl)acrylamide (LQM330),* **Figure S20.** *FT-IR spectrum of (E)-N-Phenyl-3-(4-(trifluoromethyl)phenyl)acrylamide (LQM330),* **Figure S21.** *^{1}H NMR spectrum of (E)-N-Phenyl-3-(4-(trifluoromethyl)phenyl)acrylamide (LQM330),* **Figure S22.** *^{13}C NMR spectrum of (E)-N-Phenyl-3-(4-(trifluoromethyl)phenyl)acrylamide (LQM330),* **Figure S23**. *HPLC chromatogram of (E)-3-(2,3-Dichlorophenyl)-N-phenylacrylamide (LQM331),* **Figure S24.** *FT-IR spectrum of (E)-3-(2,3-Dichlorophenyl) -N-phenylacrylamide (LQM331),* **Figure S25.** *^{1}H NMR spectrum of (E)-3-(2,3-Dichlorophenyl)-N-phenylacrylamide (LQM331),* **Figure S26**. *^{13}C NMR spectrum of (E)-3-(2,3-Dichlorophenyl)-N-phenylacrylamide (LQM331),* **Figure S27**. *HPLC chromatogram of (E)-3-(4-Fluorophenyl)-N-phenylacrylamide (LQM332),* **Figure S28.** *FT-IR spectrum of (E)-3-(4 -Fluorophenyl)-N-phenylacrylamide (LQM332),* **Figure S29.** *^{1}H NMR spectrum of (E)-3-(4-Fluorophenyl)-N -phenylacrylamide (LQM332),* **Figure S30.** *^{13}C NMR spectrum of (E)-3-(4-Fluorophenyl)-N-phenylacrylamide (LQM332),* **Figure S31.** *HPLC chromatogram of (E)-3-(2,4-Dichlorophenyl)-N-phenylacrylamide (LQM333),* **Figure S32.** *FT-IR spectrum of (E)-3-(2,4-Dichlorophenyl)-N-phenylacrylamide (LQM333),* **Figure S33**. *^{1}H NMR spectrum of (E)-3-(2,4-Dichlorophenyl)-N-phenylacrylamide (LQM333),* **Figure S34.** *^{13}C NMR spectrum of (E)-3-(2,4-Dichlorophenyl)-N -phenylacrylamide (LQM333),* **Figure S35.** *HPLC chromatogram of (E)-3-(3-Chlorophenyl)-N-phenylacrylamide (LQM334),* **Figure S36**. *FT-IR spectrum of (E)-3-(3-Chlorophenyl)-N-phenylacrylamide (LQM334),* **Figure S37.** *^{1}H NMR spectrum of (E)-3-(3-Chlorophenyl)-N-phenylacrylamide (LQM334),* **Figure S38.** *^{13}C NMR spectrum of (E)-3-(3-Chlorophenyl)-N -phenylacrylamide (LQM334),* **Figure S39.** *HPLC chromatogram of (E)-3-(3,4-Dimethoxyphenyl)-N-phenylacrylamide (LQM335),* **Figure S40**. *FT-IR spectrum of (E)-3-(3,4-Dimethoxyphenyl)-N-phenylacrylamide (LQM335),* **Figure S41.** *^{1}H NMR spectrum of (E)-3-(3,4-Dimethoxyphenyl)-N-phenylacrylamide (LQM335),* **Figure S42**. *^{13}C NMR spectrum of (E)-3-(3,4-Dimethoxyphenyl)-N-phenylacrylamide (LQM335),* **Figure S43.** *HPLC chromatogram of (E)-3-(2-Methoxyphenyl)-N-phenylacrylamide (LQM336),* **Figure S44.** *FT-IR spectrum of (E)-3-(2-Methoxyphenyl) -N-phenylacrylamide (LQM336),* **Figure S45.** *^{1}H NMR spectrum of (E)-3-(2-Methoxyphenyl)-N-phenylacrylamide (LQM336),* **Figure S46**. *^{13}C NMR spectrum of (E)-3-(2-Methoxyphenyl)-N-phenylacrylamide (LQM336),* **Figure S47.** *HPLC chromatogram of (E)-3-([1,1′-Biphenyl]-2-yl)-N-phenylacrylamide (LQM337),* **Figure S48.** *FT-IR spectrum of (E)-3-([1,1′-Biphenyl]-2-yl)-N-phenylacrylamide (LQM337),* **Figure S49.** *^{1}H NMR spectrum of (E)-3-([1,1′-Biphenyl]-2-yl) -N-phenylacrylamide (LQM337),* **Figure S50.** *^{13}C NMR spectrum of (E)-3-([1,1′-Biphenyl]-2-yl)-N-phenylacrylamide (LQM337).*

Author Contributions: All the authors have contributed to making this work possible. In this context, G.F.S.P. and M.G.M.G. synthesized all the acrylamide derivatives and characterized all of them by using

FT-IR spectrophotometry, melting point, and elemental analysis; Professors J.X.d.A.-J. and T.M.d.A. performed the structural characterization of acrylamides by using NMR spectroscopy and HPLC; S.J.M.d.S. and J.P.M.C. performed cytotoxicity and antiviral assays; E.C.d.S. performed the flow cytometry experiment; Ê.J.B. was responsible to supervise all biological experiments (cytotoxicity, antiviral, and flow cytometry), and also he wrote these correspondent sections in this manuscript; E.F.d.S.-J. organized the complete workflow of this work, rationally designed all acrylamide analogs by performing in silico methods (dynamics simulations and molecular docking), and supervised all activities associated with synthesis and chemical characterization of these compounds. Finally, he wrote these corresponding sections in this manuscript. All authors have read and agreed to the published version of the manuscript.

Funding: National Council for Scientific and Technological Development (CNPq) grant number 437407/2018-7.

Acknowledgments: The authors thank to Coordenação de Aperfeiçoamento Pessoal de Nível Superior (CAPES), National Council for Scientific and Technological Development (CNPq), Fundação de Amparo à Pesquisa do Estado de Alagoas (FAPEAL), and Financier of Studies and Projects (FINEP) for their support to the Post-Graduate Programs in Pharmaceutical Sciences (PPGCF), and Chemistry and Biotechnology (PPGQB). Also, the authors thank to organizers and conference committee from the 5th International Electronic Conference on Medicinal Chemistry (5-ECMC), especially to the Dr. Jean Jacques Vanden Eynde from the University of Mons—Belgium, for his support during the role event. Finally, the authors also acknowledge the website https://smart.servier.com by providing sources to generate the graphical abstract.

Conflicts of Interest: The authors have no relevant affiliations or financial involvement with any organization or entity with a financial interest in or financial conflict with the subject matter or materials discussed in the manuscript. This includes employment, consultancies, honoraria, stock ownership or options, expert testimony, grants or patents received or pending, or royalties. Finally, the authors declare no conflict of interest.

References

1. Pietilä, M.K.; Hellström, K.; Ahola, T. Alphavirus polymerase and RNA replication. *Virus Res.* **2017**, *234*, 44–57. [CrossRef] [PubMed]
2. Da Silva-Júnior, E.F.; Leoncini, G.O.; Rodrigues, É.E.S.; Aquino, T.M.; Araújo-Júnior, J.X. The medicinal chemistry of Chikungunya virus. *Bioorg. Med. Chem.* **2017**, *25*. [CrossRef] [PubMed]
3. Abdelnabi, R.; Amrun, S.N.; Ng, L.F.P.; Leyssen, P.; Neyts, J.; Delang, L. Protein kinases C as potential host targets for the inhibition of chikungunya virus replication. *Antivir. Res.* **2017**, *139*, 79–87. [CrossRef] [PubMed]
4. Rodríguez-Morales, A.J.; Cardona-Ospina, J.A.; Fernanda Urbano-Garzón, S.; Sebastian Hurtado-Zapata, J. Prevalence of Post-Chikungunya Infection Chronic Inflammatory Arthritis: A Systematic Review and Meta-Analysis. *Arthritis Care Res.* **2016**. [CrossRef] [PubMed]
5. Eleftheriadou, I.; Dieringer, M.; Poh, X.Y.; Sanchez-Garrido, J.; Gao, Y.; Sgourou, A.; Simmons, L.E.; Mazarakis, N.D. Selective transduction of astrocytic and neuronal CNS subpopulations by lentiviral vectors pseudotyped with Chikungunya virus envelope. *Biomaterials* **2017**, *123*, 1–14. [CrossRef]
6. Petersen, L.R.; Powers, A.M. Chikungunya: Epidemiology. *F1000Research* **2016**, *5*, 82. [CrossRef]
7. Villamil-Gómez, W.E.; Rodriguez-Morales, A.J. Reply: Dengue RT-PCR-positive, Chikungunya IgM-positive and Zika RT-PCR-positive co-infection in a patient from Colombia. *J. Infect. Public Health* **2017**, *10*, 133–134. [CrossRef]
8. Wang, Y.; Liu, X. Stability and Hopf bifurcation of a within-host chikungunya virus infection model with two delays. *Math. Comput. Simul.* **2017**, *138*, 31–48. [CrossRef]
9. Mayer, S.V.; Tesh, R.B.; Vasilakis, N. The emergence of arthropod-borne viral diseases: A global prospective on dengue, chikungunya and zika fevers. *Acta Trop.* **2017**, *166*, 155–163. [CrossRef]
10. Younger, D.S. Epidemiology of Zika Virus. *Neurol. Clin.* **2016**, *34*, 1049–1056. [CrossRef]
11. Riou, J.; Poletto, C.; Boëlle, P.-Y. A comparative analysis of Chikungunya and Zika transmission. *Epidemics* **2017**, *19*, 43–52. [CrossRef] [PubMed]
12. Van Aalst, M.; Nelen, C.M.; Goorhuis, A.; Stijnis, C.; Grobusch, M.P. Long-term sequelae of chikungunya virus disease: A systematic review. *Travel Med. Infect. Dis.* **2017**, *15*, 8–22. [CrossRef] [PubMed]
13. Amraoui, F.; Failloux, A.-B. Chikungunya: An unexpected emergence in Europe. *Curr. Opin. Virol.* **2016**, *21*, 146–150. [CrossRef] [PubMed]
14. Hwang, J.; Jiang, A.; Fikrig, E. A potent prolyl tRNA synthetase inhibitor antagonizes Chikungunya and Dengue viruses. *Antivir. Res.* **2019**, *161*, 163–168. [CrossRef]

15. Lee, H.; Halverson, S.; Ezinwa, N. Mosquito-Borne Diseases. *Prim. Care Clin. Off. Pract.* **2018**, *45*, 393–407. [CrossRef]
16. WHO. Chikungunya—Key Facts. Available online: https://www.who.int/news-room/fact-sheets/detail/chikungunya (accessed on 8 March 2020).
17. Couderc, T.; Gangneux, N.; Chretien, F.; Caro, V.; Le Luong, T.; Ducloux, B.; Tolou, H.; Lecuit, M.; Grandadam, M. Chikungunya Virus Infection of Corneal Grafts. *J. Infect. Dis.* **2012**, *206*, 851–859. [CrossRef]
18. Singh, S.K.; Unni, S.K. Chikungunya virus: Host pathogen interaction. *Rev. Med. Virol.* **2011**, *21*, 78–88. [CrossRef]
19. Thiberville, S.-D.; Moyen, N.; Dupuis-Maguiraga, L.; Nougairede, A.; Gould, E.A.; Roques, P.; de Lamballerie, X. Chikungunya fever: Epidemiology, clinical syndrome, pathogenesis and therapy. *Antivir. Res.* **2013**, *99*, 345–370. [CrossRef]
20. Behnam, M.A.M.; Nitsche, C.; Boldescu, V.; Klein, C.D. The Medicinal Chemistry of Dengue Virus. *J. Med. Chem.* **2016**, *59*, 5622–5649. [CrossRef]
21. Shrinet, J.; Srivastava, P.; Sunil, S. Transcriptome analysis of Aedes aegypti in response to mono-infections and co-infections of dengue virus-2 and chikungunya virus. *Biochem. Biophys. Res. Commun.* **2017**, *492*, 617–623. [CrossRef]
22. Prata-Barbosa, A.; Cleto-Yamane, T.L.; Robaina, J.R.; Guastavino, A.B.; de Magalhães-Barbosa, M.C.; de Moraes Brindeiro, R.; Medronho, R.A.; da Cunha, A.J.L.A. Co-infection with Zika and Chikungunya viruses associated with fetal death—A case report. *Int. J. Infect. Dis.* **2018**, *72*, 25–27. [CrossRef] [PubMed]
23. Da Silva-Júnior, E.F.; de Araújo-Júnior, J.X. Peptide derivatives as inhibitors of NS2B-NS3 protease from Dengue, West Nile, and Zika flaviviruses. *Bioorg. Med. Chem.* **2019**, *27*, 3963–3978. [CrossRef]
24. Silva-Júnior, E.F.; Schirmeister, T.; Araújo-Júnior, J.X. Recent Advances in Inhibitors of Flavivirus NS2B-NS3 Protease from Dengue, Zika, and West Nile Viruses. In *Vector-Borne Diseases & Treatment*, 1st ed.; Open Access eBooks: Las Vegas, NV, USA, 2018; Volume 2, pp. 1–25.
25. Hotez, P.J. Ten failings in global neglected tropical diseases control. *PLoS Negl. Trop. Dis.* **2017**, *11*, e0005896. [CrossRef] [PubMed]
26. Bonifay, T.; Douine, M.; Bonnefoy, C.; Hurpeau, B.; Nacher, M.; Djossou, F.; Epelboin, L. Poverty and Arbovirus Outbreaks: When Chikungunya Virus Hits More Precarious Populations Than Dengue Virus in French Guiana. *Open Forum Infect. Dis.* **2017**, *4*, ofx247. [CrossRef]
27. Moloo, A. *Neglected Tropical Diseases*; World Health Organization: Geneva, Switzerland, 2020.
28. Bourjot, M.; Delang, L.; Nguyen, V.H.; Neyts, J.; Guéritte, F.; Leyssen, P.; Litaudon, M. Prostratin and 12-O-tetradecanoylphorbol 13-acetate are potent and selective inhibitors of chikungunya virus replication. *J. Nat. Prod.* **2012**, *75*, 2183–2187. [CrossRef] [PubMed]
29. Javelle, E.; Gautret, P.; Ribéra, A.; Gaüzère, B.A.; Cabié, A.; Corail, P.R.; Simon, F. The challenge of chronic chikungunya. *Travel Med. Infect. Dis.* **2017**, *15*, 3–4. [CrossRef]
30. Plante, K.; Wang, E.; Partidos, C.D.; Weger, J.; Gorchakov, R.; Tsetsarkin, K.; Borland, E.M.; Powers, A.M.; Seymour, R.; Stinchcomb, D.T.; et al. Novel chikungunya vaccine candidate with an ires-based attenuation and host range alteration mechanism. *PLoS Pathog.* **2011**, *7*, e100214. [CrossRef]
31. Gigante, A.; Canela, M.-D.; Delang, L.; Priego, E.-M.; Camarasa, M.-J.; Querat, G.; Neyts, J.; Leyssen, P.; Pérez-Pérez, M.-J. Identification of [1,2,3]triazolo[4,5-d]pyrimidin-7(6H)-ones as novel inhibitors of Chikungunya virus replication. *J. Med. Chem.* **2014**, *57*, 4000–4008. [CrossRef]
32. Jain, J.; Dubey, S.K.; Shrinet, J.; Sunil, S. Dengue Chikungunya co-infection: A live-in relationship?? *Biochem. Biophys. Res. Commun.* **2017**, *492*, 608–616. [CrossRef]
33. Liu, X.; Thomas, C.E.; Felder, C.C. The impact of external innovation on new drug approvals: A retrospective analysis. *Int. J. Pharm.* **2019**, *563*, 273–281. [CrossRef]
34. Burt, F. Chikungunya: A re-emerging virus. *Lancet* **2012**, *379*, 662–671. [CrossRef]
35. Rashad, A.A.; Mahalingam, S.; Keller, P.A. Chikungunya virus: Emerging targets and new opportunities for medicinal chemistry. *J. Med. Chem.* **2014**, *57*, 1147–1166. [CrossRef] [PubMed]
36. Schwartz, O.; Albert, M.L. Biology and pathogenesis of chikungunya virus. *Nat. Rev. Microbiol.* **2010**, *8*, 491–500. [CrossRef] [PubMed]
37. Saisawang, C.; Kuadkitkan, A.; Smith, D.R.; Ubol, S.; Ketterman, A.J. Glutathionylation of chikungunya nsP2 protein affects protease activity. *Biochim. Biophys. Acta Gen. Subj.* **2016**, *1861*, 106–111. [CrossRef] [PubMed]

38. Seyedi, S.S.; Shukri, M.; Hassandarvish, P.; Oo, A.; Shankar, E.M.; Abubakar, S.; Zandi, K. Computational Approach Towards Exploring Potential Anti-Chikungunya Activity of Selected Flavonoids. *Sci. Rep.* **2016**, *6*, 24027. [CrossRef] [PubMed]
39. Russo, A.T.; Malmstrom, R.D.; White, M.A.; Watowich, S.J. Structural basis for substrate specificity of alphavirus nsP2 proteases. *J. Mol. Graph. Model.* **2010**, *29*, 46–53. [CrossRef] [PubMed]
40. Bhakat, S.; Karubiu, W.; Jayaprakash, V.; Soliman, M.E.S. A perspective on targeting non-structural proteins to combat neglected tropical diseases: Dengue, West Nile and Chikungunya viruses. *Eur. J. Med. Chem.* **2014**, *87*, 677–702. [CrossRef]
41. Kaur, P.; Chu, J.J.H. Chikungunya virus: An update on antiviral development and challenges. *Drug Discov. Today* **2013**, *18*, 969–983. [CrossRef]
42. Tsetsarkin, K.A.; Chen, R.; Weaver, S.C. Interspecies transmission and chikungunya virus emergence. *Curr. Opin. Virol.* **2016**, *16*, 143–150. [CrossRef]
43. Blaising, J.; Polyak, S.J.; Pécheur, E.I. Arbidol as a broad-spectrum antiviral: An update. *Antivir. Res.* **2014**, *107*, 84–94. [CrossRef]
44. Scuotto, M.; Abdelnabi, R.; Collarile, S.; Schiraldi, C.; Delang, L.; Massa, A.; Ferla, S.; Brancale, A.; Leyssen, P.; Neyts, J.; et al. Discovery of novel multi-target indole-based derivatives as potent and selective inhibitors of chikungunya virus replication. *Bioorg. Med. Chem.* **2017**, *25*, 327–337. [CrossRef] [PubMed]
45. Tsetsarkin, K.A.; McGee, C.E.; Volk, S.M.; Vanlandingham, D.L.; Weaver, S.C.; Higgs, S. Epistatic roles of E2 glycoprotein mutations in adaption of Chikungunya virus to Aedes albopictus and Ae. Aegypti mosquitoes. *PLoS ONE* **2009**, *4*, e6835. [CrossRef] [PubMed]
46. Sourisseau, M.; Schilte, C.; Casartelli, N.; Trouillet, C.; Guivel-Benhassine, F.; Rudnicka, D.; Sol-Foulon, N.; Le Roux, K.; Prevost, M.C.; Fsihi, H.; et al. Characterization of reemerging chikungunya virus. *PLoS Pathog.* **2007**, *3*, e89. [CrossRef] [PubMed]
47. Bala Murugan, S.; Sathishkumar, R. Chikungunya infection: A potential re-emerging global threat. *Asian Pac. J. Trop. Med.* **2016**, *9*, 933–937. [CrossRef] [PubMed]
48. Jadav, S.S.; Jayaprakash, V.; Basu, A.; Sinha, B.N. Chikungunya Protease Domain—High throughput Virtual Screening. *Int. J. Pharmacol. Pharm. Sci.* **2012**, *6*, 1765–1768. [CrossRef]
49. Nguyen, P.T.V.; Yu, H.; Keller, P.A. Journal of Molecular Graphics and Modelling Identification of chikungunya virus nsP2 protease inhibitors using structure-base approaches. *J. Mol. Graph. Model.* **2015**, *57*, 1–8. [CrossRef]
50. Lucas-Hourani, M.; Lupan, A.; Desprès, P.; Thoret, S.; Pamlard, O.; Dubois, J.; Guillou, C.; Tangy, F.; Vidalain, P.O.; Munier-Lehmann, H. A phenotypic assay to identify chikungunya virus inhibitors targeting the nonstructural protein nsP2. *J. Biomol. Screen.* **2013**, *18*, 172–179. [CrossRef]
51. Jadav, S.S.; Sinha, B.N.; Hilgenfeld, R.; Pastorino, B.; De Lamballerie, X.; Jayaprakash, V. Thiazolidone derivatives as inhibitors of chikungunya virus. *Eur. J. Med. Chem.* **2015**, *89*, 172–178. [CrossRef]
52. Singh, H.; Mudgal, R.; Narwal, M.; Kaur, R.; Singh, V.A.; Malik, A.; Chaudhary, M.; Tomar, S. Chikungunya virus inhibition by peptidomimetic inhibitors targeting virus-specific cysteine protease. *Biochimie* **2018**, *149*, 51–61. [CrossRef]
53. Ching, K.-C.; Tran, T.N.Q.; Amrun, S.N.; Kam, Y.-W.; Ng, L.F.P.; Chai, C.L.L. Structural Optimizations of Thieno[3,2-b]pyrrole Derivatives for the Development of Metabolically Stable Inhibitors of Chikungunya Virus. *J. Med. Chem.* **2017**, *60*, 3165–3186. [CrossRef]
54. Ching, K.-C.; Kam, Y.-W.; Merits, A.; Ng, L.F.P.; Chai, C.L.L. Trisubstituted Thieno[3,2-b]pyrrole 5-Carboxamides as Potent Inhibitors of Alphaviruses. *J. Med. Chem.* **2015**, *58*, 9196–9213. [CrossRef] [PubMed]
55. Yoon, J.; Kim, G.; Jarhad, D.B.; Kim, H.-R.; Shin, Y.-S.; Qu, S.; Sahu, P.K.; Kim, H.O.; Lee, H.W.; Wang, S.B.; et al. Design, Synthesis, and Anti-RNA Virus Activity of 6′-Fluorinated-Aristeromycin Analogues. *J. Med. Chem.* **2019**, *62*, 6346–6362. [CrossRef] [PubMed]
56. Bassetto, M.; De Burghgraeve, T.; Delang, L.; Massarotti, A.; Coluccia, A.; Zonta, N.; Gatti, V.; Colombano, G.; Sorba, G.; Silvestri, R.; et al. Computer-aided identification, design and synthesis of a novel series of compounds with selective antiviral activity against chikungunya virus. *Antivir. Res.* **2013**, *98*, 12–18. [CrossRef]

57. Giancotti, G.; Cancellieri, M.; Balboni, A.; Giustiniano, M.; Novellino, E.; Delang, L.; Neyts, J.; Leyssen, P.; Brancale, A.; Bassetto, M. Rational modifications on a benzylidene-acrylohydrazide antiviral scaffold, synthesis and evaluation of bioactivity against Chikungunya virus. *Eur. J. Med. Chem.* **2018**, *149*, 56–68. [CrossRef]
58. Das, P.K.; Puusepp, L.; Varghese, F.S.; Utt, A.; Ahola, T.; Kananovich, D.G.; Lopp, M.; Merits, A.; Karelson, M. Design and validation of novel chikungunya virus protease inhibitors. *Antimicrob. Agents Chemother.* **2016**, *60*, 7382–7395. [CrossRef] [PubMed]
59. Tardugno, R.; Giancotti, G.; De Burghgraeve, T.; Delang, L.; Neyts, J.; Leyssen, P.; Brancale, a.; Bassetto, M. Design, synthesis and evaluation against Chikungunya virus of novel small-molecule antiviral agents. *Bioorg. Med. Chem.* **2018**, *26*, 869–874. [CrossRef]
60. Di Mola, A.; Peduto, A.; La Gatta, A.; Delang, L.; Pastorino, B.; Neyts, J.; Leyssen, P.; de Rosa, M.; Filosa, R. Structure-activity relationship study of arbidol derivatives as inhibitors of chikungunya virus replication. *Bioorg. Med. Chem.* **2014**, *22*, 6014–6025. [CrossRef]
61. Sangeetha, K.; Purushothaman, I.; Rajarajan, S. Spectral characterisation, antiviral activities, in silico ADMET and molecular docking of the compounds isolated from Tectona grandis to chikungunya virus. *Biomed. Pharmacother.* **2017**, *87*, 302–310. [CrossRef]
62. Feibelman, K.M.; Fuller, B.P.; Li, L.; Labarbera, D.V.; Brian, J. Identification of small molecule inhibitors of the Chikungunya virus nsP1 RNA capping enzyme. *Antivir. Res.* **2018**. [CrossRef]
63. Wada, Y.; Orba, Y.; Sasaki, M.; Kobayashi, S.; Carr, M.J.; Nobori, H.; Sato, A.; Hall, W.W.; Sawa, H. Discovery of a Novel Antiviral Agent Targeting the Nonstructural Protein 4 (nsP4) of Chikungunya Virus. *Virology* **2017**, *505*, 102–112. [CrossRef]
64. Rathore, A.P.S.; Haystead, T.; Das, P.K.; Merits, A.; Ng, M.L.; Vasudevan, S.G. Chikungunya virus nsP3 & nsP4 interacts with HSP-90 to promote virus replication: HSP-90 inhibitors reduce CHIKV infection and inflammation in vivo. *Antivir. Res.* **2014**. [CrossRef]
65. Khan, M.; Dhanwani, R.; Patro, I.K.; Rao, P.V.L.; Parida, M.M. Cellular IMPDH enzyme activity is a potential target for the inhibition of Chikungunya virus replication and virus induced apoptosis in cultured mammalian cells. *Antivir. Res.* **2011**, *89*, 1–8. [CrossRef]
66. Strauss, E.G.; Groot, R.J.; Levinson, R.; Strauss, J.H. Identification of the active site residues in the nsP2 proteinase of Sindbis virus. *Virology* **1992**, *191*, 932–940. [CrossRef]
67. Dar, A.M.; Mir, S. Molecular Docking: Approaches, Types, Applications and Basic Challenges. *J. Anal. Bioanal. Tech.* **2017**, *8*, 356. [CrossRef]
68. Pagadala, N.S.; Syed, K.; Tuszynski, J. Software for molecular docking: A review. *Biophys. Rev.* **2017**, *9*, 91–102. [CrossRef] [PubMed]
69. Salmaso, V.; Moro, S. Bridging molecular docking to molecular dynamics in exploring ligand-protein recognition process: An overview. *Front. Pharmacol.* **2018**, *9*, 923. [CrossRef] [PubMed]
70. Guariento, S.; Bruno, O.; Fossa, P.; Cichero, E. New insights into PDE4B inhibitor selectivity: CoMFA analyses and molecular docking studies. *Mol. Divers.* **2016**, *20*, 77–92. [CrossRef] [PubMed]
71. Cichero, E.; Cesarini, S.; Spallarossa, A.; Mosti, L.; Fossa, P. Acylthiocarbamates as non-nucleoside HIV-1 reverse transcriptase inhibitors: Docking studies and ligand-based CoMFA and CoMSIA analyses. *J. Mol. Model.* **2009**, *15*, 871–884. [CrossRef]
72. Korb, O.; Stützle, T.; Exner, T.E. Empirical scoring functions for advanced Protein-Ligand docking with PLANTS. *J. Chem. Inf. Model.* **2009**, *49*, 84–96. [CrossRef]
73. Trott, O.; Olson, A. AutoDock Vina: Improving the speed and accuracy of docking with a new scoring function, efficient optimization and multithreading. *J. Comput. Chem.* **2010**, *31*, 455–461. [CrossRef]
74. Pouliot, M.; Jeanmart, S. Pan Assay Interference Compounds (PAINS) and Other Promiscuous Compounds in Antifungal Research. *J. Med. Chem.* **2016**, *59*, 497–503. [CrossRef] [PubMed]
75. Verma, G.; Marella, A.; Shaquiquzzaman, M.; Marella, A.; Akhtar, M.; Ali, M. A review exploring biological activities of hydrazones. *J. Pharm. Bioallied Sci.* **2014**, *6*, 69. [CrossRef] [PubMed]
76. Zacuto, M.J. Synthesis of Acrylamides via the Doebner–Knoevenagel Condensation. *J. Org. Chem.* **2019**, *84*, 6465–6474. [CrossRef]
77. Olawode, E.O.; Tandlich, R.; Prinsloo, E.; Isaacs, M.; Hoppe, H.; Seldon, R.; Warner, D.F.; Steenkamph, V.; Kaye, P.T. Synthesis and biological evaluation of (E)-cinnamic acid, (E)-2-styrylthiazole and (E)-2-[2-(naphthalen-1-yl)vinyl]thiazole derivatives. *Arkivoc* **2017**, *2016*, 284–296. [CrossRef]

78. Jacobsen, N.E. *NMR Data Interpretation Explained—Understanding 1D and 2D NMR Spectra of Organic Compounds and Natural Products*, 1st ed.; John Wiley & Sons Ltd.: Hoboken, NJ, USA, 2017; pp. 1–656.
79. Millies, B.; von Hammerstein, F.; Gellert, A.; Hammerschmidt, S.; Barthels, F.; Göppel, U.; Immerheiser, M.; Elgner, F.; Jung, N.; Basic, M.; et al. Proline-Based Allosteric Inhibitors of Zika and Dengue Virus NS2B/NS3 Proteases. *J. Med. Chem.* **2019**, *62*, 11359–11382. [CrossRef]
80. Mosmann, T. Rapid colorimetric assay for cellular growth and survival: Application to proliferation and cytotoxicity assays. *J. Immunol. Methods* **1983**, *65*, 55–63. [CrossRef]
81. Ramírez, D.; Caballero, J. Is It Reliable to Take the Molecular Docking Top Scoring Position as the Best Solution without Considering Available Structural Data? *Molecules* **2018**, *23*, 1038. [CrossRef]
82. Mena-Ulecia, K.; Tiznado, W.; Caballero, J. Study of the Differential Activity of Thrombin Inhibitors Using Docking, QSAR, Molecular Dynamics, and MM-GBSA. *PLoS ONE* **2015**, *10*, e0142774. [CrossRef]
83. Gohlke, H.; Hendlich, M.; Klebe, G. Knowledge-based scoring function to predict protein-ligand interactions. *J. Mol. Biol.* **2000**, *295*, 337–356. [CrossRef]
84. Voss, J.E.; Vaney, M.-C.; Duquerroy, S.; Vonrhein, C.; Girard-Blanc, C.; Crublet, E.; Thompson, A.; Bricogne, G.; Rey, F.A. Glycoprotein organization of Chikungunya virus particles revealed by X-ray crystallography. *Nature* **2010**, *468*, 709–712. [CrossRef]
85. Deeba, F.; Malik, M.Z.; Naqvi, I.H.; Haider, M.S.H.; Shafat, Z.; Sinha, P.; Ishrat, R.; Ahmed, A.; Parveen, S. Potential entry inhibitors of the envelope protein (E2) of Chikungunya virus: In silico structural modeling, docking and molecular dynamic studies. *VirusDisease* **2017**, *28*, 39–49. [CrossRef] [PubMed]
86. Agarwal, G. Virtual screening of inhibitors against Envelope glycoprotein of Chikungunya Virus: A drug repositioning approach. *Bioinformation* **2019**, *15*, 439–447. [CrossRef] [PubMed]
87. Song, H.; Zhao, Z.; Chai, Y.; Jin, X.; Li, C.; Yuan, F.; Liu, S.; Gao, Z.; Wang, H.; Song, J.; et al. Molecular Basis of Arthritogenic Alphavirus Receptor MXRA8 Binding to Chikungunya Virus Envelope Protein. *Cell* **2019**, *177*, 1–11. [CrossRef] [PubMed]
88. Thompson, M. Molecular Docking Using ArgusLab: An efficient shape-based search algorithm and an enhanced XScore scoring function. In *Proceedings of The 228th ACS National Meeting*; Planaria Software LLC: Philadelphia, PA, USA, 2004.
89. Cheung, J.; Franklin, M.; Mancia, F.; Rudolph, M.; Cassidy, M.; Gary, E.; Burshtevn, F.; Love, J. Structure of the Chikungunya virus nsP2 protease. **2011**. To be published. [CrossRef]
90. Law, Y.-S.; Utt, A.; Tan, Y.B.; Zheng, J.; Wang, S.; Chen, M.W.; Griffin, P.R.; Merits, A.; Luo, D. Structural insights into RNA recognition by the Chikungunya virus nsP2 helicase. *Proc. Natl. Acad. Sci. USA* **2019**, *116*, 9558–9567. [CrossRef]
91. Malet, H.; Coutard, B.; Jamal, S.; Dutartre, H.; Papageorgiou, N.; Neuvonen, M.; Ahola, T.; Forrester, N.; Gould, E.A.; Lafitte, D.; et al. The Crystal Structures of Chikungunya and Venezuelan Equine Encephalitis Virus nsP3 Macro Domains Define a Conserved Adenosine Binding Pocket. *J. Virol.* **2009**, *83*, 6534–6545. [CrossRef]
92. Sharma, R.; Kesari, P.; Kumar, P.; Tomar, S. Structure-function insights into chikungunya virus capsid protein: Small molecules targeting capsid hydrophobic pocket. *Virology* **2018**, *515*, 223–234. [CrossRef]
93. Jones, G.; Willett, P.; Glen, R.C.; Leach, A.R.; Taylor, R. Development and validation of a genetic algorithm for flexible docking. *J. Mol. Biol.* **1997**, *267*, 727–748. [CrossRef]
94. Lozano Untiveros, K.; da Silva, E.G.; de Abreu, F.C.; da Silva-Júnior, E.F.; de Araújo-Junior, J.X.; Mendoça de Aquino, T.; Armas, S.M.; de Moura, R.O.; Mendonça-Junior, F.J.B.; Serafim, V.L.; et al. An electrochemical biosensor based on Hairpin-DNA modified gold electrode for detection of DNA damage by a hybrid cancer drug intercalation. *Biosens. Bioelectron.* **2019**, *133*, 160–168. [CrossRef]
95. Santana, C.C.; Silva-Júnior, E.F.; Santos, J.C.N.; da S. Rodrigues, É.E.; da Silva, I.M.; Araújo-Júnior, J.X.; do Nascimento, T.G.; Oliveira Barbosa, L.A.; Dornelas, C.B.; Figueiredo, I.M.; et al. Evaluation of guanylhydrazone derivatives as inhibitors of Candida rugosa digestive lipase: Biological, biophysical, theoretical studies and biotechnological application. *Bioorg. Chem.* **2019**, *87*, 169–180. [CrossRef]
96. Roque Marques, K.M.; do Desterro, M.R.; de Arruda, S.M.; de Araújo Neto, L.N.; do Carmo Alves de Lima, M.; de Almeida, S.M.V.; da Silva, E.C.D.; de Aquino, T.M.; da Silva-Júnior, E.F.; de Araújo-Júnior, J.X.; et al. 5-Nitro-Thiophene-Thiosemicarbazone Derivatives Present Antitumor Activity Mediated by Apoptosis and DNA Intercalation. *Curr. Top. Med. Chem.* **2019**, *19*, 1075–1091. [CrossRef]

97. Marques, R.A.; Gomes, A.O.C.V.; de Brito, M.V.; dos Santos, A.L.P.; da Silva, G.S.; de Lima, L.B.; Nunes, F.M.; de Mattos, M.C.; de Oliveira, F.C.E.; do Ó Pessoa, C.; et al. Annonalide and derivatives: Semisynthesis, cytotoxic activities and studies on interaction of annonalide with DNA. *J. Photochem. Photobiol. B Biol.* **2018**, *179*, 156–166. [CrossRef]
98. De M. Silva, M.; Macedo, T.S.; Teixeira, H.M.P.; Moreira, D.R.M.; Soares, M.B.P.; da C. Pereira, A.L.; de L. Serafim, V.; Mendonça-Júnior, F.J.B.; do Carmo A. de Lima, M.; de Moura, R.O.; et al. Correlation between DNA/HSA-interactions and antimalarial activity of acridine derivatives: Proposing a possible mechanism of action. *J. Photochem. Photobiol. B Biol.* **2018**, *189*, 165–175. [CrossRef]
99. Da Silva-Junior, E.F.; Barcellos Franca, P.H.; Ribeiro, F.F.; Bezerra Mendonca-Junior, F.J.; Scotti, L.; Scotti, M.T.; de Aquino, T.M.; de Araujo-Junior, J.X. Molecular Docking Studies Applied to a Dataset of Cruzain Inhibitors. *Curr. Comput. Aided. Drug Des.* **2017**, *14*, 68–78. [CrossRef] [PubMed]
100. Silva-Junior, E.F.; Barcellos Franca, P.H.; Quintans-Junior, L.J.; Mendonca-Junior, F.J.B.; Scotti, L.; Scotti, M.T.; de Aquino, T.M.; de Araujo-Junior, J.X. Dynamic Simulation, Docking and DFT Studies Applied to a Set of Anti-Acetylcholinesterase Inhibitors in the enzyme β-Secretase (BACE-1): An Important Therapeutic Target in Alzheimer's Disease. *Curr. Comput. Aided. Drug Des.* **2017**, *13*, 266–274. [CrossRef] [PubMed]
101. De Brito, W.A.; Dantas, M.G.; Nogueira, F.H.A.; Da Silva-Júnior, E.F.; De Araújo-Júnior, J.X.; De Aquino, T.M.A.D.; Ribeiro, Ê.A.N.; Da Silva Solon, L.G.; Aragão, C.F.S.; Gomes, A.P.B. Development and validation of HPLC-DAD and UHPLC-DAD methods for the simultaneous determination of guanylhydrazone derivatives employing a factorial design. *Molecules* **2017**, *22*, 1394. [CrossRef]
102. Yakoub, K.; Jung, S.; Sattler, C.; Damerow, H.; Weber, J.; Kretzschmann, A.; Cankaya, A.S.; Piel, M.; Rösch, F.; Haugaard, A.S.; et al. Structure–Function Evaluation of Imidazopyridine Derivatives Selective for δ-Subunit-Containing γ-Aminobutyric Acid Type A (GABA A) Receptors. *J. Med. Chem.* **2018**, *61*, 1951–1968. [CrossRef]
103. Cardoso, M.V.O.; Siqueira, L.R.P.; Silva, E.B.; Costa, L.B.; Hernandes, M.Z.; Rabello, M.M.; Pereira, V.R.A.; Castro, M.C.A.B.; Bernhardt, P.V.; Leite, A.C.L. 2-Pyridyl thiazoles as novel anti- Trypanosoma cruzi agents: Structural design, synthesis and pharmacological evaluation. *Eur. J. Med. Chem.* **2014**, *86*, 48–59. [CrossRef]
104. Moreira, D.R.M.; De Oliveira, A.D.T.; Teixeira De Moraes Gomes, P.A.; De Simone, C.A.; Villela, F.S.; Ferreira, R.S.; Da Silva, A.C.; Dos Santos, T.A.R.; Brelaz De Castro, M.C.A.; Pereira, V.R.A.; et al. Conformational restriction of aryl thiosemicarbazones produces potent and selective anti-Trypanosoma cruzi compounds which induce apoptotic parasite death. *Eur. J. Med. Chem.* **2014**, *75*, 467–478. [CrossRef]
105. Pretsch, E.; Bühlmann, P.; Badertscher, M. *Structure Determination of Organic Compounds—Tables of Spectral Data*, 4th ed.; Springer: Berlin/Heidelberg, Germany, 2009; pp. 1–391.
106. Silva-júnior, E.F.; Silva, E.P.S.; França, P.H.B.; Silva, J.P.N.; Barreto, E.O.; Silva, E.B.; Ferreira, R.S.; Gatto, C.C.; Moreira, D.R.M.; Siqueira-neto, J.L.; et al. Synthesis, molecular docking and biological evaluation of thiophen-2-iminothiazolidine derivatives for use against Trypanosoma cruzi. *Bioorg. Med. Chem.* **2016**, *24*, 4228–4240. [CrossRef]
107. Abo-Ashour, M.F.; Eldehna, W.M.; Nocentini, A.; Ibrahim, H.S.; Bua, S.; Abou-Seri, S.M.; Supuran, C.T. Novel hydrazido benzenesulfonamides-isatin conjugates: Synthesis, carbonic anhydrase inhibitory activity and molecular modeling studies. *Eur. J. Med. Chem.* **2018**, *157*, 28–36. [CrossRef]
108. Eldehna, W.M.; Al-Ansary, G.H.; Bua, S.; Nocentini, A.; Gratteri, P.; Altoukhy, A.; Ghabbour, H.; Ahmed, H.Y.; Supuran, C.T. Novel indolin-2-one-based sulfonamides as carbonic anhydrase inhibitors: Synthesis, in vitro biological evaluation against carbonic anhydrases isoforms I, II, IV and VII and molecular docking studies. *Eur. J. Med. Chem.* **2017**, *127*, 521–530. [CrossRef] [PubMed]
109. Allam, H.A.; Fahim, S.H.; F.Abo-Ashour, M.; Nocentini, A.; Elbakry, M.E.; Abdelrahman, M.A.; Eldehna, W.M.; Ibrahim, H.S.; Supuran, C.T. Application of hydrazino and hydrazido linkers to connect benzenesulfonamides with hydrophilic/phobic tails for targeting the middle region of human carbonic anhydrases active site: Selective inhibitors of hCA IX. *Eur. J. Med. Chem.* **2019**, *179*, 547–556. [CrossRef] [PubMed]
110. Luo, D.; Vasudevan, S.G.; Lescar, J. The flavivirus NS2B–NS3 protease–helicase as a target for antiviral drug development. *Antivir. Res.* **2015**, *118*, 148–158. [CrossRef]
111. Carissimi, M. Esters and amides of 4-biphenylylacrylic acid of possible antiphlogistic and analgesic action. II. *Farm. Ed. Sci.* **1959**, *14*, 141–145.
112. Guo, C.; Jiang, K.; Yue, L.; Xia, Z.; Wang, X.; Pan, Y. Intriguing roles of reactive intermediates in dissociation chemistry of N-phenylcinnamides. *Org. Biomol. Chem.* **2012**, *10*, 7070. [CrossRef]

113. Sethiya, J.P.; Bhavsar, S.P.; Shahare, H.V. Synthesis of Potential Anti-Inflammatory Pyrazoline Derivatives Under Ultrasonic Irradiation. *Int. J. Pharm. Sci. Res.* **2019**, *10*, 3290–3294. [CrossRef]
114. Qiu, J.; Zhang, R. Direct transformation of arylpropynes to acrylamides via a three-step tandem reaction. *Org. Biomol. Chem.* **2014**, *12*, 1556–1560. [CrossRef]
115. Fei, Z.; Zeng, C.; Lu, C.; Zhao, B.; Yao, Y. An efficient asymmetric hydrophosphonylation of unsaturated amides catalyzed by rare-earth metal amides [(Me 3 Si) 2 N] 3 RE(μ-Cl)Li(THF) 3 with phenoxy-functionalized chiral prolinols. *RSC Adv.* **2017**, *7*, 19306–19311. [CrossRef]
116. de Araújo-Vilges, K.M.; de Oliveira, S.V.; Couto, S.C.P.; Fokoue, H.H.; Romero, G.A.S.; Kato, M.J.; Romeiro, L.A.S.; Leite, J.R.S.A.; Kuckelhaus, S.A.S. Effect of piplartine and cinnamides on Leishmania amazonensis, Plasmodium falciparum and on peritoneal cells of Swiss mice. *Pharm. Biol.* **2017**, *55*, 1601–1607. [CrossRef]
117. Ittyerah, P.I.; Pandya, K.C. Condensation of malonanilic acid with aldehydes. *Proc. Indian Acad. Sci. Sect. A* **1941**, *13*, 461–466. [CrossRef]
118. Yamamori, T.; Nagata, K.; Ishizuka, N.; Sakai, K. Preparation of Aryl Amides, Arylpropenamides, and Arylpentadienamides as Promoters of Apolipoprotein AI Expression for the Treatment of Dyslipidemia and Arteriosclerotic Diseases. U.S. Patent 20040235888 A1, 21 April 2004.
119. Drayman, N.; Oppenheim, A. Rapid Titration of Viruses by Flow Cytometry. *Curr. Protoc. Cell Biol.* **2011**, *51*, 26.11.1–26.11.7. [CrossRef] [PubMed]